Available online at www.sciencedirect.com
SCIENCE DIRECT®
Journal of Sound and Vibration 285 (2005) 517–546
JOURNAL OF SOUND AND VIBRATION
www.elsevier.com/locate/jsvi

Autoparametric resonances in a structure/fluid interaction system carrying a cylindrical liquid tank

Takashi Ikeda*, Shin Murakami

Department of Electronic and Control Systems Engineering, Shimane University, 1060 Nishikawatsu, Matsue 690-8504, Japan

Received 5 August 2003; received in revised form 10 August 2004; accepted 26 August 2004
Available online 25 November 2004

Abstract

The nonlinear-coupled vibrations of an elastic structure and liquid sloshing in a cylindrical container are investigated. The behavior of the liquid surface is governed by a kind of the Mathieu equation because the structure is subjected to a vertical and sinusoidal excitation. Modal equations for liquid sloshing governing the coupled motions are derived when the natural frequency of the structure is equal to twice the natural frequency of an anti-symmetric mode of sloshing. The theoretical resonance curves are determined by using van der Pol's method. The influences of a liquid level and a detuning parameter on the theoretical resonance curves are investigated when only the excitation frequency is selected as a control parameter. The inclination of a frequency response curve depends on the liquid level. Furthermore, a small deviation of the tuning condition may cause amplitude- and phase-modulated motions and chaotic vibrations. This deviation also leads to separate the occurrence region of the coupled vibration into two regions of the excitation frequency. The theoretical resonance curves are quantitatively in agreement with the experimental data. Lastly, the amplitude- and phase-modulated motions and chaotic vibrations were observed in experiments.

*Corresponding author. Tel.: +81 852 32 8908; fax: +81 852 32 8909.
E-mail address: tikeda@riko.shimane-u.ac.jp (T. Ikeda).

0022-460X/$ - see front matter © 2004 Elsevier Ltd. All rights reserved.
doi:10.1016/j.jsv.2004.08.015

Nomenclature

c	damping coefficient of the structure
F_l	vertical fluid force
F_0	amplitude of excitation
g	acceleration of gravity
h	depth of the liquid
k	spring constant of the structure
M	summation of masses of the structure and the liquid ($=m+m_l$)
m	mass of the structure
m_l	mass of the liquid
P	fluid pressure
p_0	natural frequency of the structure (or the main system)
p_{mn}	natural frequency of the (m,n) sloshing mode (m,n: integers)
R	tank radius
(r,θ,z)	circular cylindrical coordinate system (see Fig. 1)
t	time
(x,y,z)	rectangular coordinate system (see Fig. 1)
z_0	displacement of the structure
η	displacement of the liquid surface
$v_1=m/M$	
$v_2=m_lR/(\pi Mh)$	
ρ	fluid density
ϕ	velocity potential
ω	excitation frequency
ζ_{mn}	damping ratios of (m,n) sloshing mode

1. Introduction

Vibrations of an elastic structure with liquid containers are very important problems from the viewpoint of structure performance and disaster prevention. Associated problems often appear in industry such as elevated water tanks and liquefied natural gas (LNG) tanks. When the motion of a liquid surface—referred to as sloshing—occurs in containers, the nonlinearity of the liquid inertia force essentially appears. Therefore, this nonlinearity must be taken into account to accurately analyze the dynamic behavior of the liquid sloshing. Liquid sloshing dynamics including free and forced free-surface motions, sloshing interaction with elastic structures, numerical techniques, and sloshing under low gravitational field are reviewed elsewhere [1].

Many papers examined the nonlinear behavior of liquid sloshing in circular cylindrical containers that are excited harmonically. However, most of these deal with the case of a horizontal excitation [2–5], while few papers have examined a vertical excitation [6–8]. Interaction problems of an elastic structure and a liquid sloshing—which are the main subjects of this paper—have primarily focused on tuned liquid dampers. Regarding the damping effects that circular cylindrical liquid tanks have on the vibration of the structure under horizontal excitation, Senda and Nakagawa [9] were early to report on linear analysis. Since then, experimental [10,11] and nonlinear analyses [12,13] have also been reported. On the other hand, few papers have dealt with interaction problems where a structure is subjected to vertical excitation for a rectangular tank [14] and a circular cylindrical tank [15–18]. The authors of this paper examined the case where an axisymmetric sloshing mode was excited in a circular cylindrical tank [18] and improving the accuracy of the former analysis [15] by considering multiple sloshing modes. However, as two different modes of an identical natural frequency are degenerated, the behavior of an anti-symmetrical sloshing mode in a cylindrical tank becomes more complicated than that of the case of an axisymmetric mode.

This paper presents the theoretical and experimental resonance curves when an elastic structure carrying a circular cylindrical liquid tank is subjected to a vertical sinusoidal excitation. The only nonlinearity that exists here is due to the large amplitude of liquid sloshing. In the theoretical analysis, the modal equations—which govern the dynamic behavior of coupled vibrations between the structure and the liquid sloshing of an anti-symmetric mode—have been derived by using van der Pol's method [19] at the 2:1 internal resonance ratio. The influences of the liquid levels and the deviation of the internal resonance ratio on the theoretical resonance curves are investigated when only the excitation frequency is selected as a control parameter. The experiments have demonstrated that the theoretical resonance curves are quantitatively in agreement with the experimental ones.

2. Theoretical analysis

2.1. Equations of motion

Ibrahim and his co-researchers [15–17] have adopted an elastic structure with a cylindrical liquid container where the structure can move in both horizontal and vertical directions. In this study, however, practical structures, such as towers and buildings, are modeled as a single-degree-of-freedom (sdof) system provisioning only vertical movement, which makes the system and the essence of coupled vibrations between the structure and the liquid sloshing much easier to understand.

A model for theoretical analysis is shown in Fig. 1. We consider an sdof system as a structure, which consists of the mass m, the spring with spring constant k, and the dashpot with damping coefficient c. This structure is subjected to a vertical sinusoidal excitation. A circular cylindrical partially filled tank with a radius R and depth h is supported by the structure. Let us consider a moving rectangular coordinate system (x, y, z) and a circular cylindrical coordinate system (r, θ, z), which are fixed on the tank. The xy-plane coincides with the undisturbed surface of the liquid. The vertical displacement of the mass m, measured from its equilibrium position, is designated as z_0. The elevation of the liquid surface at the position of (r, θ) is η. Damping effects due to the fluid viscosity essentially influence the behavior of the liquid sloshing. Therefore, the Navier–Stokes equation should be undertaken in order to precisely analyze the viscous fluid. However, it is rather difficult to solve this equation. Here the following procedure is adopted. Namely, the linear viscous damping terms are added to the modal equations in a phenomenological way after all the transformations have been completed by using potential flow theory. Here, the velocity potential ϕ of the liquid particles, moving relative to the tank, is introduced. The Laplace equation (i.e., the continuity equation) is given in terms of ϕ:

$$\Delta\phi(r, \theta, z, t) \equiv \frac{\partial^2\phi}{\partial r^2} + \frac{1}{r}\frac{\partial\phi}{\partial r} + \frac{1}{r^2}\frac{\partial^2\phi}{\partial\theta^2} + \frac{\partial^2\phi}{\partial z^2} = 0 \tag{1}$$

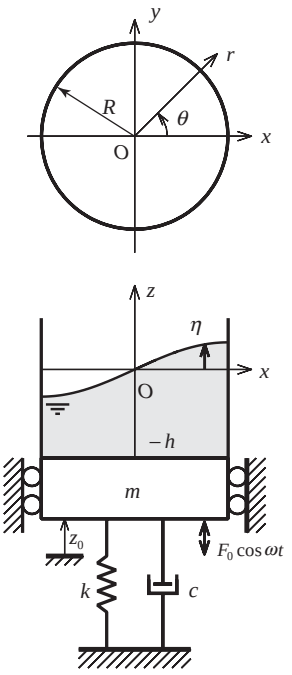

Fig. 1. The model for theoretical analysis.

and the generalized Bernoulli equation (i.e., the pressure equation) is given in Refs. [15,20,21] as

$$\frac{\partial\phi}{\partial t}+\frac{1}{2}\left\{\left(\frac{\partial\phi}{\partial r}\right)^2+\frac{1}{r^2}\left(\frac{\partial\phi}{\partial\theta}\right)^2+\left(\frac{\partial\phi}{\partial z}\right)^2\right\}+gz+\frac{P}{\rho}=-\ddot{z}_0 z, \tag{2}$$

where $P(r,\theta,z,t)$ is the fluid pressure, ρ is the fluid density, g is the acceleration of gravity and the symbol "$\cdot$" represents the derivative with respect to the time t.

When the structure is vertically subjected to the sinusoidal excitation $F_0\cos\omega t$, the equation of motion for the structure is

$$m\ddot{z}_0+c\dot{z}_0+kz_0=F_l+F_0\cos\omega t+m_l g, \tag{3}$$

where F_l is the fluid force acting in the z direction on the structure through the tank bottom, and m_l is the mass of liquid. The third term on the right-hand side of Eq. (3) is produced because of the definition of the equilibrium position of z_0. The fluid force F_l is given by

$$F_l=-\int_0^{2\pi}\int_0^R rP(r,\theta,z,t)|_{z=-h}\,\mathrm{d}r\,\mathrm{d}\theta, \tag{4}$$

where $P(r,\theta,z,t)$ is given by Eq. (2).

Now the following dimensionless quantities are defined as

$$z_0' = z_0/R, \quad \eta' = \eta/R, \quad r' = r/R, \quad z' = z/R, \quad h' = h/R, \quad v_1 = m/M, \quad v_2 = m_l/(\pi M h'),$$
$$\phi' = \phi/(R^2 p_{11}), \quad k' = k/(M p_{11}^2), \quad c' = c/(M p_{11}), \quad F' = F/(MR p_{11}^2),$$
$$F_l' = F_l/(MR p_{11}^2), \quad P' = P/(\rho R^2 p_{11}^2), \quad t' = p_{11} t, \quad \xi_{mn} = \lambda_{mn} R,$$
$$[M = m + m_l, \quad p_{11} = \sqrt{g\lambda_{11}\tanh(\lambda_{11} h)}]. \tag{5}$$

Note that the quantities in the parenthesis [ ] in Eq. (5) have dimensions. The quantity λ_{mn} denotes the nth positive root in order of magnitude and satisfies the characteristic equation

$$\frac{\mathrm{d}}{\mathrm{d}r}\{J_m(\lambda r)\} = 0 \quad (\text{at } r = R), \tag{6}$$

where J_m indicates the mth order Bessel function of the first kind. The subscript (m, n) of λ_{mn} corresponds to the natural mode of liquid sloshing, where m represents the number of diametral nodal lines and n represents the order to a nodal concentric circle. For example, p_{11}, obtained from λ_{11} in Eq. (5), means the natural frequency of $(1, 1)$ mode of sloshing. Using Eq. (5) for Eqs. (1)–(4) to be written in a dimensionless form yields:

$$\phi_{rr} + \frac{1}{r}\phi_r + \frac{1}{r^2}\phi_{\theta\theta} + \phi_{zz} = 0, \tag{7}$$

$$\phi_t + \frac{1}{2}\left(\phi_r^2 + \frac{1}{r^2}\phi_\theta^2 + \phi_z^2\right) + \frac{1}{\psi_{11}} z + P = -\ddot{z}_0 z, \tag{8}$$

$$v_1 \ddot{z}_0 + c\dot{z}_0 + k z_0 = F_l + F_0 \cos\omega t + v_2 \pi h/\psi_{11}, \tag{9}$$

$$F_l = -v_2 \int_0^{2\pi} \int_0^1 r P(r, \theta, z, t)|_{z=-h}\, \mathrm{d}r\, \mathrm{d}\theta, \tag{10}$$

where $\psi_{11} = \xi_{11}\tanh(\xi_{11} h)$ and the symbols "′" designating dimensionless quantities are all omitted. The subscripts r, θ, z and t, as seen in ϕ_r, ϕ_{rr}, $\phi_{\theta\theta}$, etc., represent the partial differentiation with respect to the corresponding coordinates.

Because the fluid velocities vanish at the side walls and bottom of the tank, the boundary conditions for ϕ are given by

$$\phi_r = 0 \quad (\text{at } r = 1), \quad \phi_z = 0 \quad (\text{at } z = -h). \tag{11}$$

Next, because the vertical velocity of the fluid particle on the liquid surface is equal to the velocity of the liquid surface in the vertical direction, one can obtain the kinematic boundary condition [15]

$$\phi_z = \eta_t + \phi_r \eta_r + \frac{1}{r^2}\phi_\theta \eta_\theta \quad (\text{at } z = \eta). \tag{12}$$

Moreover, because $P = 0$ at the free surface $z = \eta$, the boundary condition for Eq. (8) is given by

$$\phi_t + \frac{1}{2}\left(\phi_r^2 + \frac{1}{r^2}\phi_\theta^2 + \phi_z^2\right) + \frac{1}{\psi_{11}} z = -\ddot{z}_0 z \quad (\text{at } z = \eta). \tag{13}$$

2.2. Unstable regions in the corresponding linear system

In this section, the boundaries of the unstable regions will be determined by using the corresponding linear system. In terms of the eigenfunctions obtained from a free vibration analysis, the solutions of ϕ and η are assumed as follows:

$$\phi(r,\theta,z,t) = a_c(t) + \sum_{m=0}^{\infty}\sum_{n=1}^{\infty}\{a_{mn}(t)\cos\, m\theta + b_{mn}(t)\sin\, m\theta\}J_m(\xi_{mn}r)\cosh\{\xi_{mn}(z+h)\}/\cosh(\xi_{mn}h), \tag{14a}$$

$$\eta(r,\theta,t) = \sum_{m=0}^{\infty}\sum_{n=1}^{\infty}\{c_{mn}(t)\cos m\theta + d_{mn}(t)\sin m\theta\}J_m(\xi_{mn}r), \tag{14b}$$

where a_c, a_{mn}, b_{mn}, c_{mn} and d_{mn} are the unknown functions of time. Among those, c_{mn} and d_{mn} represent the amplitudes of the (m,n) sloshing mode. The mode shapes of the natural vibrations of sloshing with $m=0$ are axisymmetric about the z-axis and other mode shapes are all anti-symmetric. The term a_c in Eq. (14a) is important upon determining the fluid force in the nonlinear analysis, discussed in Section 2.3. However, the constant term is not necessary in Eq. (14b) because the undisturbed liquid surface coincides with the x-axis (i.e., $z=0$).

Figs. 2(a)–(c) show the shapes of natural vibrations for $(0,1)$, $(1,1)$ and $(2,1)$ modes. When $m\neq 0$, they have an identical shape for given values of m and n though the modes corresponding to $c_{mn}\cos m\theta\, J_m(\xi_{mn}r)$ and $d_{mn}\sin m\theta\, J_m(\xi_{mn}r)$ in Eq. (14b) have diametral nodal lines whose locations are different from each other by angular position $\pi/(2m)$. Therefore, b_{mn} and d_{mn} are assumed to be zero; it will then be sufficient to consider only amplitudes a_{mn} and c_{mn} in the following analysis in this section. By substituting Eq. (14) into Eq. (9) and into Eqs. (12) and (13) without nonlinear terms, and then putting $z=0$ and eliminating a_{mn}, it yields the following two kinds of equations:

$$(v_1 + v_2\pi h)\ddot{z}_0 + c\dot{z}_0 + kz_0 - 2\pi v_2\sum_{n=1}^{\infty}\frac{J_1(\xi_{0n})}{\psi_{0n}\xi_{0n}\cosh(\xi_{0n}h)}\ddot{c}_{0n} = F_0\cos\omega t, \tag{15a}$$

$$\ddot{c}_{mn} + 2\zeta_{mn}\omega_{mn}\dot{c}_{mn} + \omega_{mn}^2(1+\psi_{11}\ddot{z}_0)c_{mn} = 0, \tag{15b}$$

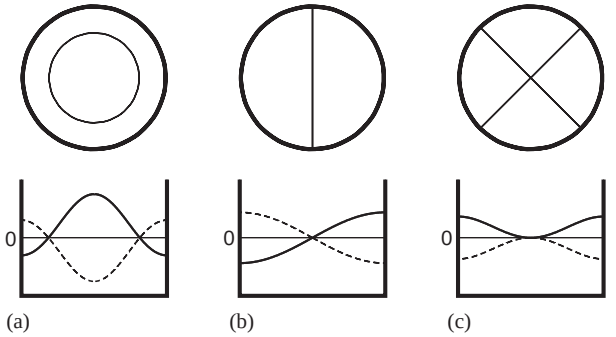

Fig. 2. Shapes of sloshing modes: (a) (0,1) mode; (b) (1,1) mode; (c) (2,1) mode.

where $\omega_{mn}^2 = \psi_{mn}/\psi_{11}$ and $\psi_{mn} = \xi_{mn}\tanh(\xi_{mn}h)$. ω_{mn} represents the natural frequency of sloshing mode (m,n) in a dimensionless form. In order to consider the damping effects of sloshing, a linear viscous damping term $2\zeta_{mn}\omega_{mn}\dot{c}_{mn}$ is added to Eq. (15b); ζ_{mn} is the damping ratio for the sloshing mode (m,n). The amplitude of c_{mn} vanishes in the stable region. However, even in the unstable regions, c_{mn} is infinitesimal in the vicinity of initial states of time. This can also be applied to the term $\ddot{c}_{0n}$ in Eq. (15a). Therefore, assuming the solution of forced oscillation for Eq. (15a) is

$$z_0 = Z\cos(\omega t + \beta) \tag{16}$$

yields the amplitude Z and the phase angle β as follows:

$$Z = \frac{F_0}{\sqrt{\{k - (v_1 + v_2\pi h)\omega^2\}^2 + (c\omega)^2}}, \tag{17a}$$

$$\beta = -\tan^{-1}\left[\frac{c\omega}{k - (v_1 + v_2\pi h)\omega^2}\right]. \tag{17b}$$

Next, substituting Eq. (16) into Eq. (15b) and adopting the time transformation

$$\tau = \omega t + \beta \tag{18}$$

yields

$$\frac{\mathrm{d}^2 c_{mn}}{\mathrm{d}\tau^2} + \mu_{mn}\frac{\mathrm{d}c_{mn}}{\mathrm{d}\tau} + (\delta_{mn} - \varepsilon_{mn}\cos\tau)c_{mn} = 0, \tag{19}$$

where $\mu_{mn} = 2\zeta_{mn}\omega_{mn}/\omega$, $\delta_{mn} = \psi_{mn}/(\psi_{11}\omega^2)$ and $\varepsilon_{mn} = \psi_{mn}Z$. Because Eq. (19) includes a parametrically excited term, it falls into the Mathieu equation. Therefore, some unstable vibrations may occur depending on the values of parameters. Periodic oscillations appear on the boundaries between the stable and unstable regions. The oscillations of frequencies $\{(2i-1)/2\}\omega\,(i = 1,2,3,\ldots,)$ are designated by using the symbol $[\{(2i-1)/2\}\omega]$. This kind of oscillation can occur on the boundary in the parameter space, which is approximately given by

$$\begin{vmatrix} 9 - 4\delta_{mn} & 2\varepsilon_{mn} & 0 & -6\mu_{mn} \\ 2\varepsilon_{mn} & 1 - 4\delta_{mn} + 2\varepsilon_{mn} & -2\mu_{mn} & 0 \\ 0 & 2\mu_{mn} & 1 - 4\delta_{mn} - 2\varepsilon_{mn} & 2\varepsilon_{mn} \\ 6\mu_{mn} & 0 & 2\varepsilon_{mn} & 9 - 4\delta_{mn} \end{vmatrix} = 0. \tag{20}$$

In addition, periodic oscillations of frequency $i\omega$ $(i = 1,2,3,\ldots,)$ may appear. However, this kind of vibration is not treated here because their unstable regions are relatively narrower compared with the width of the unstable regions depicted in Eq. (20).

2.3. Modal equations

In this section, the ordinary differential equations (referred to as modal equations) including the nonlinear terms for the amplitudes of dominant components are derived. Here, the natural frequency of the structure system [expressed by Eq. (9)] is defined as $p_0 = \sqrt{k/(v_1 + \pi v_2 h)}$. The response of the nonlinear-coupled system in the vicinity of $p_0 \cong \omega$ is investigated in the presence of the condition of internal resonance $p_0 \cong 2p_{11}$ between the natural frequencies p_0 and p_{11}. Here,

p_{11} is defined in Eq. (5) and represents the natural frequency of (1, 1) mode of liquid sloshing. Eqs. (14a) and (14b) are also used as the solutions of ϕ and η, respectively. Upon introducing the small parameter ε, the orders of the amplitudes and the damping coefficients are assumed as follows:

$$\begin{aligned} &a_{11}, b_{11}, c_{11}, d_{11}, z_0; c, \zeta_{mn} \approx O(\varepsilon^{1/3}),\\ &a_c, a_{01}, c_{01}, a_{21}, b_{21}, c_{21}, d_{21} \approx O(\varepsilon^{2/3}),\\ &a_{31}, b_{31}, c_{31}, d_{31} \approx O(\varepsilon^{3/3}). \end{aligned} \tag{21}$$

The orders of the other amplitudes, which are not shown in Eq. (21), are assumed to be smaller than $O(\varepsilon)$. The procedure to assume the orders of unknown variables in Eq. (21) is based on the following idea. When the relationship $p_0 \cong 2p_{11} \cong \omega$ is satisfied, it is found from the experimental data that the displacement z_0 of the structure and the amplitudes c_{11} and d_{11} of sloshing mod (1, 1) occur predominantly. These amplitudes, through the nonlinear terms, produce smaller ones, such as $a_c, a_{01}, c_{01}, a_{21}, b_{21}, c_{21}$ and d_{21}, and moreover, the resultant amplitudes produce much smaller ones. Because this nonlinear analysis is considered within the accuracy of the order $O(\varepsilon)$, it follows in a phenomenological way that one should assume the most predominant amplitude to be $O(\varepsilon^{1/3})$, and consecutively produced amplitudes to be $O(\varepsilon^{2/3})$. In addition, it is possible for this system to have other internal resonances depending on parameter values, as shown in Appendix C; for example, $p_0 \cong 2p_{11} \cong p_{02} \cong p_{22}$. However, a one-to-one internal resonance is not significant unless the magnitude of excitation amplitude is large [22]. Therefore, in the present case, as the excitation amplitude is not so large as to cause other internal resonances, they are not considered in this paper.

Expanding Eqs. (12) and (13) at $\eta = 0$, considering η to be small, and then substituting Eq. (14) into them, one equates the constant terms and the coefficients of $J_0(\xi_{01}r)$, $J_m(\xi_{m1}r)\cos m\theta$ and $J_m(\xi_{m1}r)\sin m\theta$ $(m = 1, 2)$ on the both sides of these equations by using the assumption in Eq. (21). In addition, substituting the pressure P from Eq. (8) into Eq. (10) and carrying out the integration, one obtains the modal equations as follows:

$$Q_1\ddot{z}_0 + c\dot{z}_0 + kz_0 + Q_2\dot{a}_c + G_1(a_{11}, b_{11}) = F_0\cos\omega t, \tag{22a}$$

$$\dot{a}_{11} + \left(1/\psi_{11} + \ddot{z}_0\right)c_{11} + G_2(\dot{a}_{i1}, \dot{b}_{j1}, a_{i1}, b_{j1}, c_{i1}, d_{j1}) = 0, \tag{22b}$$

$$\dot{b}_{11} + \left(1/\psi_{11} + \ddot{z}_0\right)d_{11} + G_3(\dot{a}_{i1}, \dot{b}_{j1}, a_{i1}, b_{j1}, c_{i1}, d_{j1}) = 0, \tag{22c}$$

$$\dot{c}_{11} - \psi_{11}a_{11} + G_4(a_{i1}, b_{j1}, c_{i1}, d_{j1}) = 0, \tag{22d}$$

$$\dot{d}_{11} - \psi_{11}b_{11} + G_5(a_{i1}, b_{j1}, c_{i1}, d_{j1}) = 0, \tag{22e}$$

$$\dot{a}_c + G_6(\dot{a}_{11}, \dot{b}_{11}, \dot{z}_0, a_{11}, b_{11}, c_{11}, d_{11}) = 0, \tag{22f}$$

$$\dot{a}_{01} + \left(1/\psi_{11} + \ddot{z}_0\right)c_{01} + G_7(\dot{a}_{11}, \dot{b}_{11}, a_{11}, b_{11}, c_{11}, d_{11}) = 0, \tag{22g}$$

$$\dot{c}_{01} - \psi_{01}a_{01} + G_8(a_{11}, b_{11}, c_{11}, d_{11}) = 0, \tag{22h}$$

$$\dot{a}_{21} + \left(1/\psi_{11} + \ddot{z}_0\right)c_{21} + G_9(\dot{a}_{11}, \dot{b}_{11}, a_{11}, b_{11}, c_{11}, d_{11}) = 0, \tag{22i}$$

$$\dot{b}_{21} + \left(1/\psi_{11} + \ddot{z}_0\right) d_{21} + G_{10}(\dot{a}_{11}, \dot{b}_{11}, a_{11}, b_{11}, c_{11}, d_{11}) = 0, \tag{22j}$$

$$\dot{c}_{21} - \psi_{21} a_{21} + G_{11}(a_{11}, b_{11}, c_{11}, d_{11}) = 0, \tag{22k}$$

$$\dot{d}_{21} - \psi_{21} b_{21} + G_{12}(a_{11}, b_{11}, c_{11}, d_{11}) = 0, \tag{22l}$$

where $Q_1 = v_1 + v_2 \pi h$, and $Q_2 = -v_2 \pi$. The term G_k $(k = 1, 2, \ldots, 12)$ represents the nonlinear terms which consist of variables a_{mn} $(m = 0, 1, 2;\ n = 1)$, b_{mn} $(m = 1, 2;\ n = 1)$, etc., shown in their parentheses (see Appendix A). Eliminating a_c from Eqs. (22a) and (22f), one obtains

$$Q_1 \ddot{z}_0 + c\dot{z}_0 + k z_0 + G_{13}(\dot{a}_{11}, \dot{b}_{11}, a_{11}, b_{11}, c_{11}, d_{11}) = F_0 \cos \omega t, \tag{23}$$

where G_{13} is given in Appendix A.

Using Eq. (21) to eliminate a_{mn} and b_{mn} from Eqs. (22b–e, g–l) and (23), and retaining the terms up to $O(\varepsilon)$, one obtains

$$Q_1 \ddot{z}_0 + c\dot{z}_0 + k z_0 + H_1(\ddot{z}_0, \dot{c}_{11}, \dot{d}_{11}, c_{11}, d_{11}) = F_0 \cos \omega t, \tag{24a}$$

$$\ddot{c}_{11} + 2\zeta_{11}\dot{c}_{11} + (1 + \psi_{11}\ddot{z}_0) c_{11} + H_2(\dot{c}_{i1}, \dot{d}_{j1}, c_{i1}, d_{j1}) = 0, \tag{24b}$$

$$\ddot{d}_{11} + 2\zeta_{11}\dot{d}_{11} + (1 + \psi_{11}\ddot{z}_0) d_{11} + H_3(\dot{c}_{i1}, \dot{d}_{j1}, c_{i1}, d_{j1}) = 0, \tag{24c}$$

$$\ddot{c}_{01} + 2\zeta_{01}\omega_{01}\dot{c}_{01} + \omega_{01}^2 (1 + \psi_{11}\ddot{z}_0) c_{01} + H_4(\ddot{z}_0, \dot{c}_{11}, \dot{d}_{11}, c_{11}, d_{11}) = 0, \tag{24d}$$

$$\ddot{c}_{21} + 2\zeta_{21}\omega_{21}\dot{c}_{21} + \omega_{21}^2 (1 + \psi_{11}\ddot{z}_0) c_{21} + H_5(\ddot{z}_0, \dot{c}_{11}, \dot{d}_{11}, c_{11}, d_{11}) = 0, \tag{24e}$$

$$\ddot{d}_{21} + 2\zeta_{21}\omega_{21}\dot{d}_{21} + \omega_{21}^2 (1 + \psi_{11}\ddot{z}_0) d_{21} + H_6(\ddot{z}_0, \dot{c}_{11}, \dot{d}_{11}, c_{11}, d_{11}) = 0, \tag{24f}$$

where H_i $(i = 1, 2, \ldots, 6)$ represent the nonlinear terms, which are given in Appendix B. It should be noted that viscous damping terms are added in Eqs. (24) in order to consider the effect of energy dissipation on sloshing—as in Eq. (15b). Eqs. (24) enable one to simulate the coupled system numerically.

2.4. Resonance curves near the tuning frequency

FFT analysis generally demonstrates the frequency components that are predominantly involved in the time histories. Mode (1, 1) has two different degenerated modes, whose diametral nodal lines intersect at a right angle. Therefore, their amplitudes c_{11} and d_{11} can be excited simultaneously near $\omega \cong p_0 \cong 2p_{11}$. In general, however, it is found from the results of numerical simulation that the diametral nodal line of sloshing mode (1, 1) is stationary with time, and that the position of its nodal line depends on the initial condition. Therefore, in a phenomenological way, the resonance curves, near the tuning frequency $\omega \cong p_0 \cong 2p_{11}$, are discussed where the diametral nodal line of mode (1, 1) coincides with the y-axis. This assumption, coinciding with the y-axis, does not make any difference of response, and does not allow any losing of the general results from analysis. Accordingly, in this section, d_{mn} is assumed to be zero in Eqs. (24). Based on the result of the FFT analysis, the solutions of a forced oscillation near the tuning frequency for

Eqs. (23) and (24) can be assumed as follows:

$$\begin{aligned} z_0 &= u_1 \cos \omega t - v_1 \sin \omega t, \\ c_{11} &= u_2 \cos \tfrac{1}{2}\omega t - v_2 \sin \tfrac{1}{2}\omega t + e_1 \cos \tfrac{3}{2}\omega t - f_1 \sin \tfrac{3}{2}\omega t, \\ c_{01} &= e_2 \cos \omega t - f_2 \sin \omega t + r_0, \\ c_{21} &= e_3 \cos \omega t - f_3 \sin \omega t + r_2, \end{aligned} \tag{25}$$

where the amplitudes u_i, v_i, e_j and f_j $(i = 1, 2;\ j = 1, 2, 3)$, and the constant terms r_0 and r_2 are assumed to vary slowly with time, according to the method of van der Pol [19]. Based on Eq. (21), the amplitudes in Eq. (25) and their derivatives with respect to time are also assumed to have the orders [12,18]

$$\begin{aligned} &u_i, v_i \approx O(\varepsilon^{1/3}), \quad e_j,\ f_j, r_0, r_2 \approx O(\varepsilon^{2/3}), \\ &\dot{u}_i, \dot{v}_i \approx O(\varepsilon^{3/3}), \quad \dot{e}_j,\ \dot{f}_j, \dot{r}_0, \dot{r}_2 \approx O(\varepsilon^{4/3}), \\ &\ddot{u}_i, \ddot{v}_i \approx O(\varepsilon^{5/3}), \quad \ddot{e}_j,\ \ddot{f}_j, \ddot{r}_0, \ddot{r}_2 \approx O(\varepsilon^{2}). \end{aligned} \tag{26}$$

Substituting Eq. (25) into Eq. (24), and then equating the same frequency terms of ω, $(\frac{1}{2})\omega$ and $(\frac{3}{2})\omega$ and the constant term on both sides within an accuracy of $O(\varepsilon)$, respectively, one obtains

$$\begin{aligned} &\dot{u}_1 = K_1(u_i, v_i, e_j,\ f_j), \quad \dot{v}_1 = K_2(u_i, v_i, e_j,\ f_j), \\ &\dot{u}_2 = K_3(u_i, v_i, e_j,\ f_j, r_k), \quad \dot{v}_2 = K_4(u_i, v_i, e_j,\ f_j, r_k), \\ &e_1 = K_5(u_i, v_i), \quad f_1 = K_6(u_i, v_i), \quad e_2 = K_7(u_i, v_i), \quad f_2 = K_8(u_i, v_i), \\ &e_3 = K_9(u_i, v_i), \quad f_3 = K_{10}(u_i, v_i), \quad r_0 = K_{11}(u_i, v_i), \quad r_2 = K_{12}(u_i, v_i). \end{aligned} \tag{27}$$

Functions K_i $(i = 1, 2, \ldots, 12)$ in Eq. (27) represent the nonlinear terms which consist of the variables in their parentheses (where, $i = 1, 2;\ j = 1, 2, 3$ and $k = 0, 2$). Their concrete forms are omitted here. Eq. (27) can be reduced to a set of ordinary differential equations of the first order for the variables u_i and v_i $(i = 1, 2)$. The steady-state solutions of Eq. (27) can be obtained numerically and their stability analysis can be performed in the same manner as Ref. [12].

A comparison has been made in the nonlinear-coupled partially filled liquid system, considered an sdof system, by replacing the liquid in the container to a same mass of solid body. The dynamic behavior of this system is governed by Eq. (15a) with $c_{0n} = 0$, and the amplitude Z of its displacement z_0 is given by Eq. (17a). In Eq. (17a), $v_1 + v_2\pi h (\equiv Q_1)$ represents the dimensionless quantity corresponding to the sum $m + m_l$, hence, the sum of the structure mass and the liquid mass. Actually, $Q_1 = 1$ in the theoretical analysis.

3. Numerical results

In the numerical calculations, the values of parameters are given such that the natural frequency p_0 of the structure system is equal to twice the natural frequency p_{11} of the sloshing mode $(1, 1)$, hence, the tuning condition (or the internal resonance) $p_0 \cong 2p_{11}$ is satisfied.

Fig. 3 shows the unstable region, which is indicated by the shaded portion on the (ω, F_0) plane for the values of parameters: $v_1 = 0.87$, $v_2 = 0.034$, $k = 4.0$, $c = 0.03$, $h = 1.2$ and $\zeta_{mn} = 0.008$ at

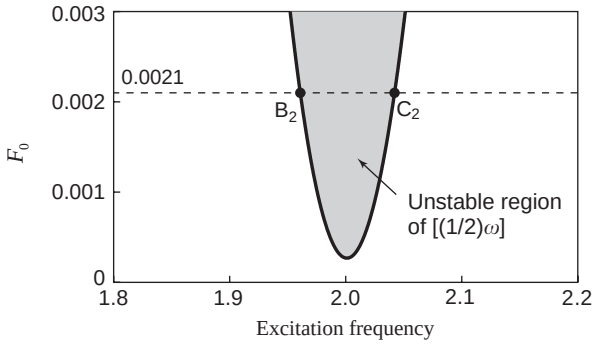

Fig. 3. Unstable region for the oscillation $[\frac{1}{2}\omega]$ of the (1,1) sloshing mode at c_{11} or d_{11}, shown by shading, when $v_1 = 0.87$, $v_2 = 0.034$, $k = 4.0$, $c = 0.03$, $h = 1.2$ and $\zeta_{mn} = 0.008$.

the oscillation $[\frac{1}{2}\omega]$ of the $(1,1)$ sloshing mode of c_{11} or d_{11}. These values are matched with the experimental apparatus A to be mentioned in Section 4. In this case, the dimensionless natural frequencies are $p_0 = 2$ and $p_{11} = 1$. The boundary of this region can be calculated by Eq. (20) with $m = 1$ and $n = 1$. It is found that the unstable region is comparatively large even if F_0 is small because the parametric excitation term $\ddot{z}_0$ in Eq. (15b) or the coefficient ε_{mn} in Eq. (19) becomes comparatively large near the resonance point of $\omega \cong p_0$. For example, the unstable vibrations of the frequency $\frac{1}{2}\omega$ occur at the interval B_2C_2 when $F_0 = 0.0021$ in Fig. 3.

3.1. Influence due to the change of liquid level

In this section, the theoretical resonance curves for three different liquid levels of the tank in the nonlinear-coupled system are demonstrated. First of all, Fig. 4 shows the steady-state time histories obtained by numerically integrating Eq. (24) with $d_{11} = 0$ and $d_{21} = 0$ through the Adams method. The initial values for z_0 and c_{mn} are 0.001. The values of the parameters, $F_0 = 0.0021$, $(r, \theta) = (1, 0)$ and $\omega = 2.03$, are in addition to those used in Fig. 3. Because d_{11} and d_{21} are always zero in Fig. 4, it is known that the diametral nodal line is located on the y-axis and a harmonic oscillation of the frequency ω in z_0 and a subharmonic oscillation of the frequency $\frac{1}{2}\omega$ in c_{11} appear predominantly.

Fig. 5 shows the result of the FFT analysis of the time histories shown in Fig. 4. For example, it can be seen clearly that the component of ω is contained in z_0, while the components of $\frac{1}{2}\omega$ and $\frac{3}{2}\omega$ in c_{11}. These results are grounds for assumption (25) for determining the resonance curves.

Resonance curves can be calculated by solving Eq. (27) numerically. Figs. 6(a) and (b) show the resonance curves for the displacement z_0 of the structure (whose amplitude is given by $\sqrt{u_1^2 + v_1^2}$) and for the amplitude c_{11} of the (1,1) sloshing mode (whose amplitude is given by $\sqrt{u_2^2 + v_2^2}$), respectively. The values of the parameters are the same as in Fig. 4. The solid line represents a stable steady-state solution, while the broken line indicates an unstable solution. The symbol "•" represents the amplitude of the frequency ω component in z_0 [shown in Fig. 6(a)] and the amplitude of the frequency $\frac{1}{2}\omega$ component in c_{11} [shown in Fig. 6(b)], which are obtained by an FFT analysis of steady-state time histories. As mentioned before, these steady-state time histories

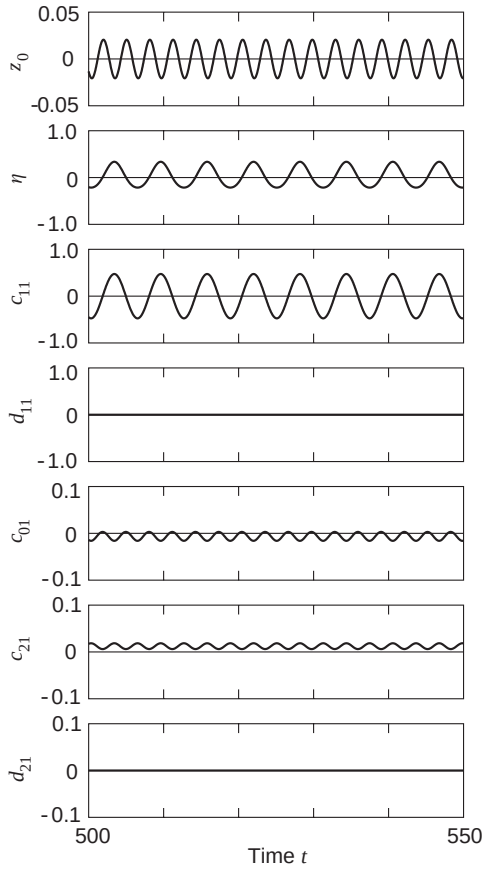

Fig. 4. Steady state time histories when $v_1 = 0.87$, $v_2 = 0.034$, $k = 4.0$, $c = 0.03$, $h = 1.2$, $\zeta_{mn} = 0.008$, $F_0 = 0.0021$, $\omega = 2.03$ and $(r, \theta) = (1, 0)$.

are calculated by directly integrating Eq. (24). It is observed that the theoretical resonance curves are in good agreement with the results of the numerical one. The branch $A_1B_1C_1D_1$ in z_0 is absolutely the same compared to the results calculated from Eq. (17a), but the branch B_1C_1 appears unstable. The corresponding branch $A_2B_2C_2D_2$ shows zero amplitude in c_{11}. In the corresponding linear system, the interval B_2C_2 results in an unstable region, as shown in Fig. 3, with divergent vibrations in this interval. In the nonlinear system, however, because the branch EF appears in Fig. 6 as a stable one, the divergent vibrations do not occur in this interval B_2C_2. Instead, a harmonic oscillation of the frequency ω and a subharmonic oscillation occur on the branch E_1F_1 and on the branch E_2F_2, respectively. When the liquid level is comparatively high as in Fig. 6, jump phenomena in amplitude appear at the points B_1 (or B_2) and E_1 (or E_2).

Figs. 7 and 8 show the theoretical resonance curves when the liquid levels are lower than in Fig. 6. The values of the parameters in Fig. 7, which differ from those in Fig. 6, are $v_1 = 0.94$, $v_2 = 0.035$, and $h = 0.55$, while they are $v_1 = 0.96$, $v_2 = 0.032$, and $h = 0.4$ in Fig. 8. Based on Fig. 6, the amplitudes of the points E_1 and F_1 in Fig. 7(a) are similar, and the amplitude

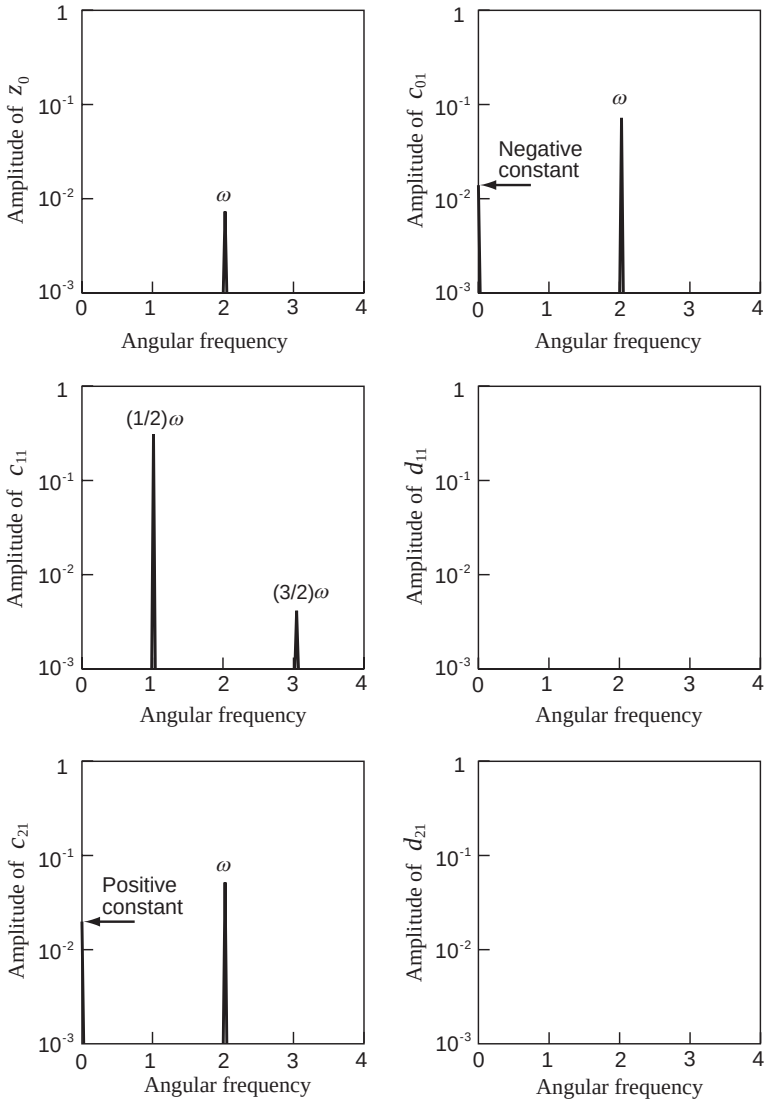

Fig. 5. FFT spectra corresponding to the time histories of Fig. 4.

of the points E_1 is larger than that of the point F_1 in Fig. 8(a). In Fig. 8, the branch BE changes to a stable solution where the point B in the Figs. 6 and 7 show the change from a subcritical pitchfork bifurcation to a supercritical one. As the liquid level decreases, the peak of the resonance curve for z_0 moves from the right side [shown by the point F_1 in Fig. 6(a)] to the left side [shown by the point E_1 in Fig. 8(a)] in the Figs. 6–8. In addition, the inclination of the resonance curve for c_{11} tends to bend toward left-hand side in Fig. 6 or toward right-hand side in Fig. 8.

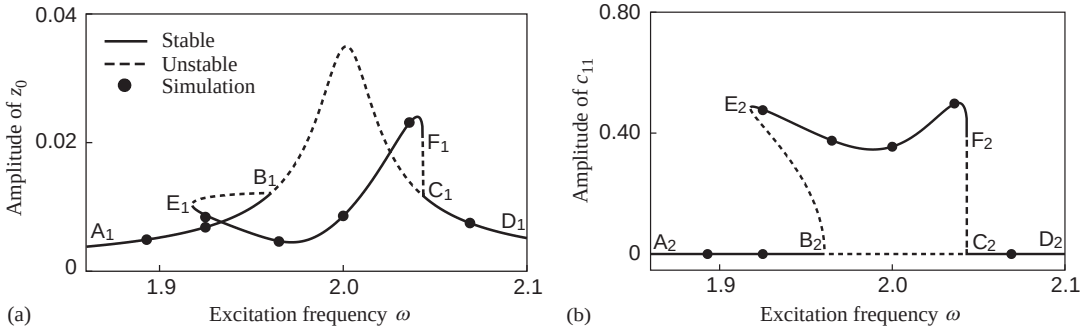

Fig. 6. Theoretical resonance curves with parameters identical to those of Fig. 4 at the high liquid level (i.e., for $h = 1.2$): (a) the amplitude of the ω component of z_0; (b) the amplitude of the $\frac{1}{2}\omega$ component of c_{11}.

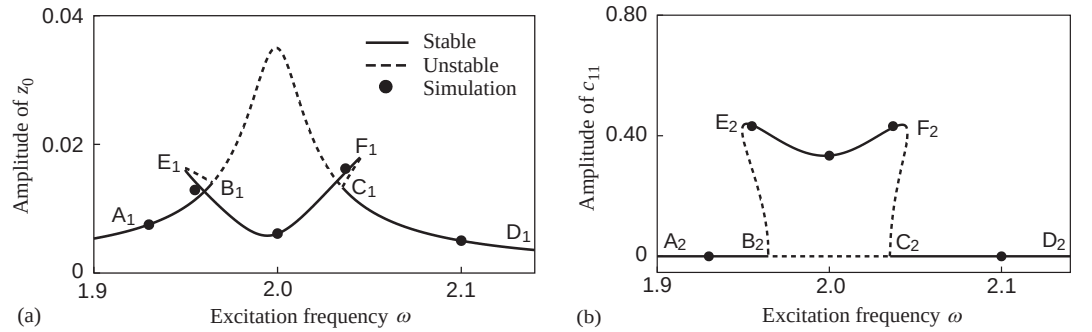

Fig. 7. Changed resonance curves from Fig. 6 when $h = 0.55$, $v_1 = 0.94$ and $v_2 = 0.035$: (a) the amplitude of the ω component of z_0; (b) the amplitude of the $\frac{1}{2}\omega$ component of c_{11}.

3.2. *Influence due to the deviation of tuning*

Next, the influence due to the deviation of the tuning condition, in particular the relationship of the internal resonance on resonance curves, is discussed. The detuning parameter is defined as $\sigma_{11} \equiv p_0 - 2p_{11}$. Fig. 9 shows the theoretical resonance curves when only the value of the spring constant k is changed from $k = 4.0$ in Fig. 6 to $k = 3.78$. This change leads to $\sigma_{11} = -0.0540$. The stable branch EF in Fig. 6 changes to an unstable interval GH on the branch EF in Fig. 9. According to the numerical simulation from Eq. (24), amplitude- and phase-modulated motions occur at the interval GH. The vertical thin lines in Fig. 9 represent the magnitude of the modulated amplitude, which are obtained from $\sqrt{z_0^2 + (\dot{z}_0/\omega)^2}$ in Fig. 9(a) and $\sqrt{c_{11}^2 + \{\dot{c}_{11}/(0.5\omega)\}^2}$ in Fig. 9(b) The location of the appearance of this amplitude- and phase-modulated motion obtained from the simulation agrees well with the theoretical analysis in this interval GH. This kind of amplitude- and phase-modulated motion also appears in other autoparametric systems such as the structures with a pendulum [23–25], the ships coupled with the

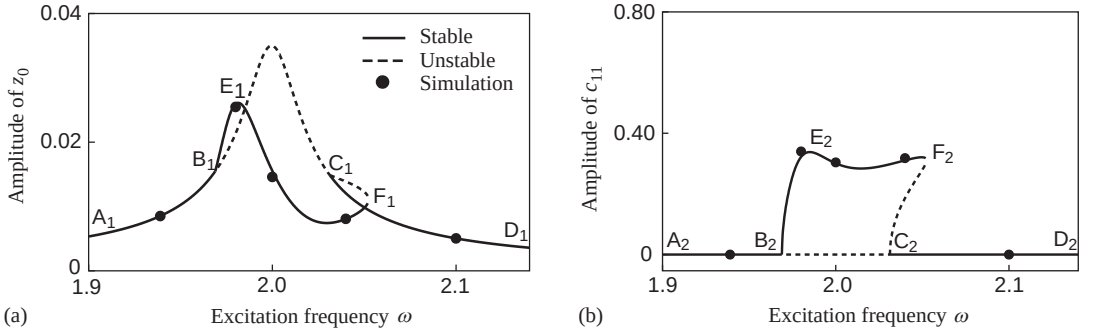

Fig. 8. Changed resonance curves from Fig. 6 when $h = 0.40$, $v_1 = 0.96$ and $v_2 = 0.032$: (a) the amplitude of the ω component of z_0; (b) the amplitude of the $\frac{1}{2}\omega$ component of c_{11}.

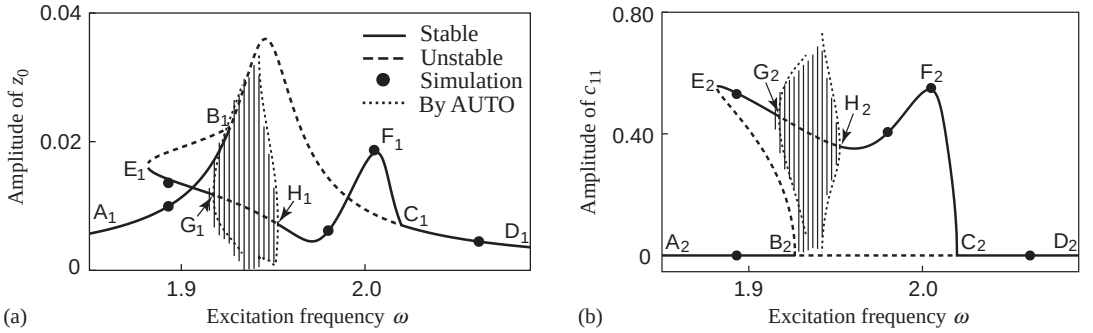

Fig. 9. Influence of the detuning parameter σ_{11} on the resonance curves; parameters are the same as Fig. 6 except for $k = 3.78$ ($\sigma_{11} = -0.0540$): (a) the amplitude of the ω component of z_0; (b) the amplitude of the $\frac{1}{2}\omega$ component of c_{11}.

pitch and roll motions [26], and an L-shaped beam with concentrated masses [27]. As mentioned in Section 2.4, Eq. (27) can be reduced to a set of ordinary differential equations of the first order for the variables u_i and v_i $(i = 1, 2)$. In this paper, numerically calculating the steady state solutions (or fixed points) from those equations, we determine their stabilities from the eigenvalues of its Jacobian matrix. For example, in Fig. 9, as the value of ω increases along the branch EF, a complex conjugate pair of eigenvalues transversely crosses the imaginary axis and other complex eigenvalues remain in the left-half plane near point G [28]. Therefore, this implies that point G is a Hopf bifurcation point. Point H is the same as point G. In addition, the simplification analyses enable one to differentiate between subcritical or supercritical type of Hopf bifurcation [29]. Here, instead of that simplification analysis, we investigate the type of these Hopf bifurcation points by applying AUTO [30] to Eq. (27). The dotted lines in Figs. 9(a) and (b) represent the maximum and minimum values of $\sqrt{\{u_1(t)\}^2 + \{v_1(t)\}^2}$ and $\sqrt{\{u_2(t)\}^2 + \{v_2(t)\}^2}$, which are the amplitudes of the orbits in the phase planes (u_1, v_1) and (u_2, v_2), when the stable periodic solutions appear at the interval GH. These dotted lines are broken off because the unusable periodic solution occurs. It is seen that those amplitudes change continuously starting

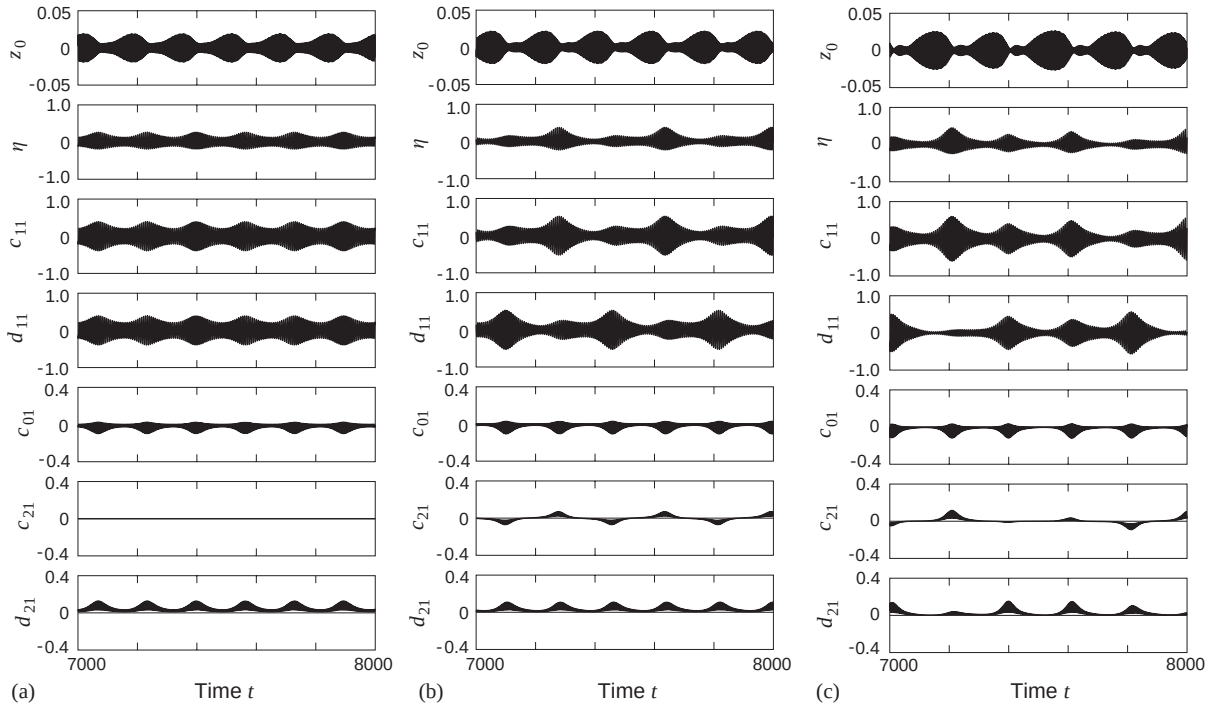

Fig. 10. Steady-state time histories at interval GH in Fig. 9 when $(r, \theta) = (1, 0)$: (a) $\omega = 1.920$; (b) $\omega = 1.925$; and (c) $\omega = 1.929$.

from points G_i and H_i $(i = 1, 2)$ without any jumps while the excitation frequency changes. Consequently, these points are found to be supercritical.

Figs. 10(a)–(c) show the steady-state time histories obtained from the numerical simulation at $\omega = 1.920$, 1.925 and 1.929 within the interval GH in Fig. 9, respectively. The initial values of d_{mn} and $\dot{d}_{mn}$ are given the same values as those of c_{mn} and $\dot{c}_{mn}$, respectively. It can be seen that the amplitude- and phase-modulated vibrations occur. The amplitude varies once, twice or irregularly in the envelope of this time history during each cycle (if it has a cycle) in Figs. 10(a)–(c), respectively. The occurrence of amplitude- and phase-modulation in Fig. 10 is not due to the liquid swirling motion because the time histories of c_{11} and d_{11} are always in phase and this implies that the nodal line of the (1, 1) sloshing mode is at rest. In order to investigate these amplitude- and phase-modulated vibrations more in detail, the Poincaré map technique is used. Figs. 11(a)–(c) show the Poincaré maps, plotted on the $(z_0, \dot{z}_0)$ plane and the $(c_{11}, \dot{c}_{11})$ plane, corresponding to Figs. 10(a)–(c) correspondingly. Poincaré maps exhibit a single-loop on the $(z_0, \dot{z}_0)$ plane and two single-loops on the $(c_{11}, \dot{c}_{11})$ plane in Fig. 11(a). They then change to two double-loops on the $(c_{11}, \dot{c}_{11})$ plane in Fig. 11(b), and finally they encounter chaotic attractors in Fig. 11(c).

To investigate the sequence up to chaotic vibrations more in detail, the Lyapunov exponents are calculated by applying the method of Wolf et al. [31] through Eq. (24). Fig. 12 shows the Lyapunov exponents, including the largest (a full line), the second largest (a broken line) and the third largest ones (a dotted line), versus the excitation frequency ω in the case of parameters as

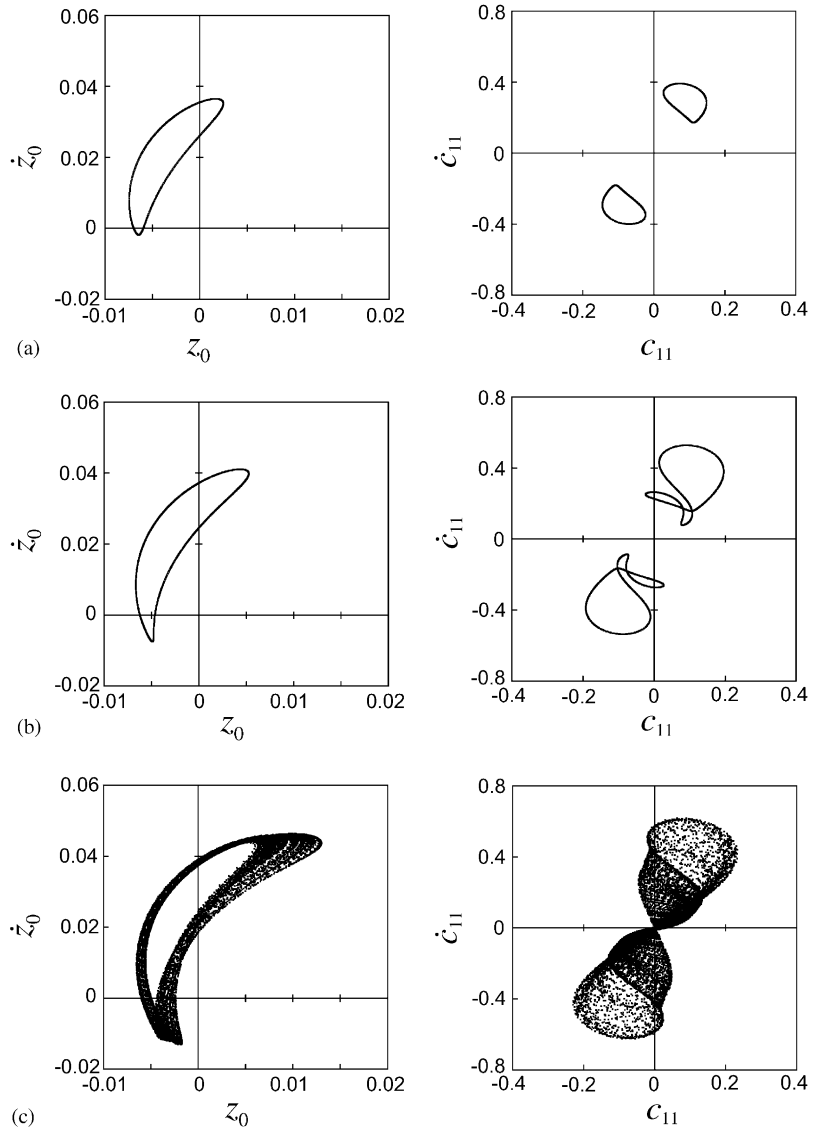

Fig. 11. Poincaré maps dotted on the $(z_0, \dot{z}_0)$ and $(c_{11}, \dot{c}_{11})$ planes corresponding to the time histories in Fig. 10: (a) $\omega = 1.920$; (b) $\omega = 1.925$; and (c) $\omega = 1.929$.

Fig. 9. The results of the largest Lyapunov exponents for the points P_a, P_b and P_c correspond to the time histories, which are shown in Figs. 11(a), (b) and (c), respectively. The points G and H represent the Hopf bifurcation points. The period-doubling bifurcation point is indicated by the point P_1. These locations are not given by the numerical results of Lyapunov exponents, but obtained by numerical simulation of Eq. (24). However, there is a strong relationship between numerical results of Eq. (24) and Lyapunov exponents. As the excitation frequency ω increases, the system experiences a Hopf bifurcation at the point G; it then encounters a period-doubling bifurcation at the point P_1. This system exhibits a chaotic behavior at the point P_c because the

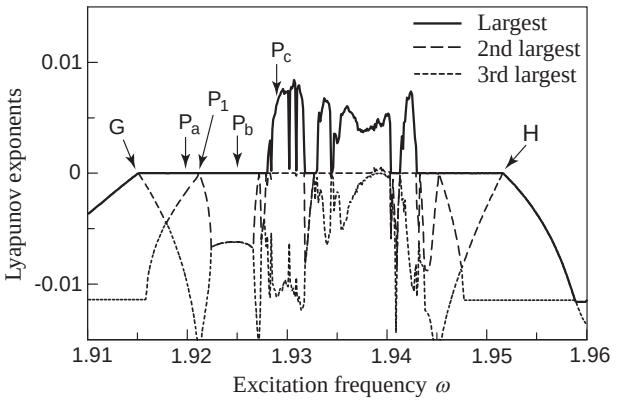

Fig. 12. Lyapunov exponents near the interval GH in Fig. 9. Points P_a, P_b and P_c represent the positions of ω corresponding to Figs. 10(a), (b) and (c), and 11(a), (b) and (c), respectively. Points G and H are Hopf bifurcation points, and P_1 is a period-doubling bifurcation point.

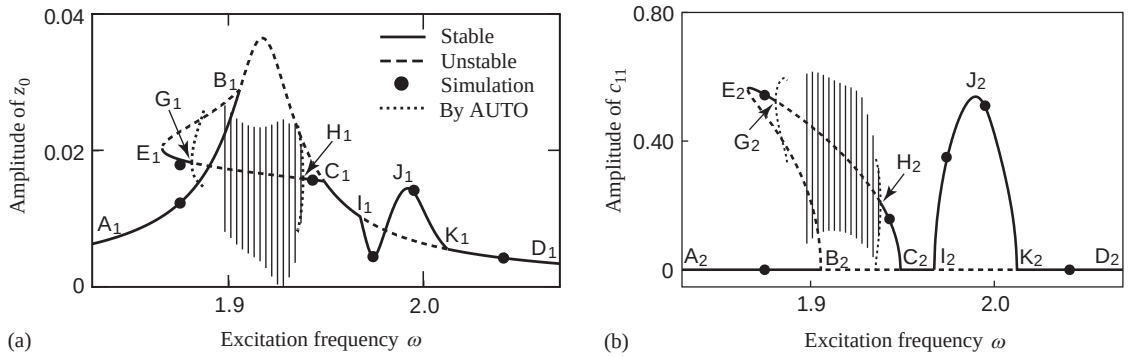

Fig. 13. Influence of the detuning parameter σ_{11} on the resonance curves for $h = 1.2$; parameters are the same as Fig. 9 except for $k = 3.67$ ($\sigma_{11} = -0.0825$): (a) the amplitude of the ω component of z_0; (b) the amplitude of the $\frac{1}{2}\omega$ component of c_{11}.

largest Lyapunov exponent is positive. In the sequence from the point P_c to the point H, depending on the value of the largest Lyapunov exponent as shown in Fig. 12, the system experiences chaotic behaviors discontinuously and returns to simply amplitude-and phase-modulated motions.

Fig. 13 shows the theoretical resonance curves when the spring constant changes from $k = 3.78$ in Fig. 9 to $k = 3.67$. This change leads to $\sigma_{11} = -0.0825$. The unstable zero-amplitude solutions of c_{11} appear in the interval I_2K_2 in addition to the interval B_2C_2, and then the nonlinear-coupled vibrations occur in the two separated regions of ω. The amplitude- and phase-modulated motions appear also on the branch BC. The dotted lines obtained by AUTO correspond to the stable periodic solutions and they are continuous near points G_i and H_i. Therefore, these points are found to be supercritical. The dotted lines are broken off because unstable periodic solutions occur. However, when σ_{11} becomes positive by changing the value of k in Fig. 9 larger, the unstable interval GH does not appear on the branch EF.

Fig. 14 shows the theoretical resonance curves where only the spring constant in Fig. 8 (for $h = 0.4$) changes to $k = 4.19$ and $\sigma_{11} = +0.0467$. It can be seen that the unstable interval GH appears and that amplitude- and phase-modulated vibrations occur in a part of the interval GH. The dotted lines are obtained by AUTO. Therefore, these Hopf bifurcation points are found to be supercritical. In this case, the dotted lines run continuously from point G to point H. This implies that the stable periodic solutions occur in the interval GH. In contrast to the case of high liquid levels, such an unstable interval as GH appears in the case of low liquid levels only when the detuning parameter σ_{11} exceeds some positive value. To be exact, it is found that this kind of amplitude- and phase-modulated vibration does not occur unless the absolute value of σ_{11} exceeds a certain threshold value, regardless of the liquid level.

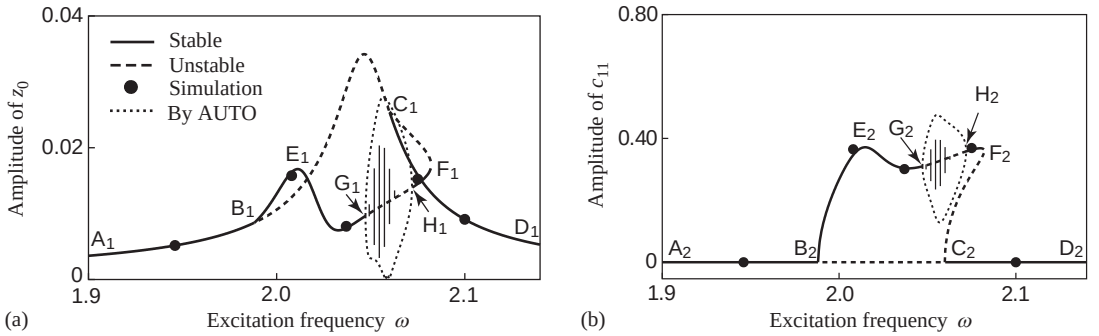

Fig. 14. Influence of the detuning parameter σ_{11} on the resonance curves for $h = 0.4$; parameters are the same as Fig. 8 except for $k = 4.19$ ($\sigma_{11} = +0.0467$): (a) the amplitude of the ω component of z_0; (b) the amplitude of the $\frac{1}{2}\omega$ component of c_{11}.

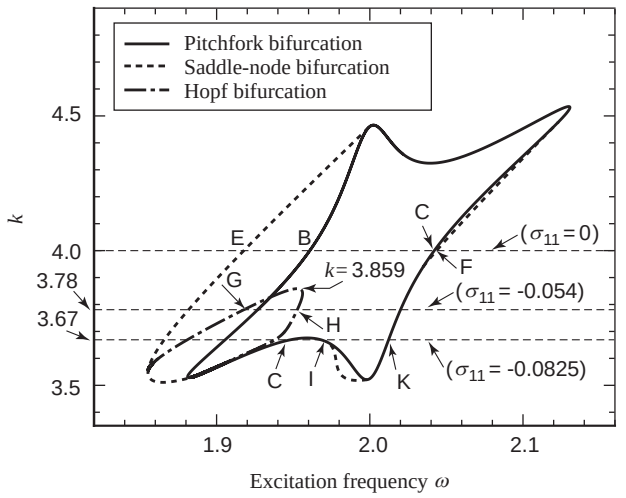

Fig. 15. Bifurcation sets in the (ω, k) parameter space for a high liquid level ($h = 1.2$), i.e., when the values of parameters are identical to those in Fig. 6 except for k.

In order to determine the appearing region of bifurcation including a pitchfork bifurcation, a saddle-node bifurcation and a Hopf bifurcation, the bifurcation sets are calculated by using AUTO. Fig. 15 shows the loci of bifurcation points (referred to as a bifurcation set), plotted on the (ω, k) control parameter space when the liquid level is high (for $h = 1.2$). Namely, this figure includes the information about bifurcation sets in Fig. 6 (for $k = 4.0$), Fig. 9 (for $k = 3.78$) and Fig. 13 (for $k = 3.67$). Therefore, it is found that the Hopf bifurcation points G and H appear when the value of k is smaller than 3.859, hence $\sigma_{11} < -0.0338$ ($\equiv \sigma_{S1}$). σ_{S1} represents a threshold value at which a Hopf bifurcation starts to appear.

The results above mentioned can be summarized as follows: In the case of high liquid levels, two Hopf bifurcation points appear on the branch of resonance curves when the detuning parameter is smaller than the threshold σ_{S1} (<0)—that is $\sigma_{11} \leqslant \sigma_{S1} < 0$. Then, amplitude- and phase-modulated vibrations occur between these bifurcation points. On the other hand, in the case of low liquid levels, amplitude- and phase-modulated vibrations occur when σ_{11} is larger than σ_{S2} (>0)—that is $\sigma_{11} \geqslant \sigma_{S2} > 0$.

4. Experimental apparatus

Fig. 16 shows the sketch of the experimental apparatus. A T-shaped structure, which was attached to the end of two 500 mm length arms with ball bearings in their joints to constrain the

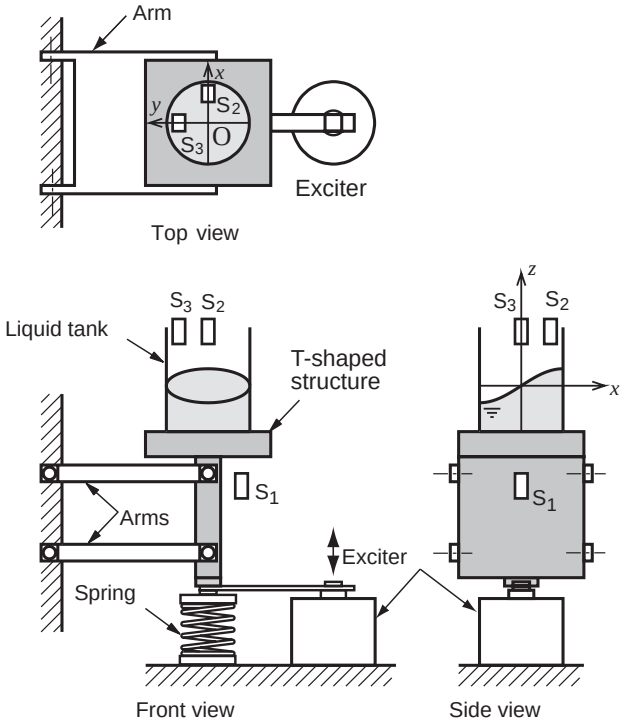

Fig. 16. The setup of the experimental apparatus.

horizontal motion, was supported by a spring at the bottom (see the front view). Therefore, this structure was able to move only in the approximately vertical direction. The structure was excited sinusoidally and stepwise at each excitation frequency by an electromagnetic exciter (Brüel & Kjær 4808) through a thin aluminum plate. The head of the exciter was controlled by a vibration exciter controller (Brüel & Kjær 1050) in order to keep the amplitude of the head constant regardless of any excitation frequency. A circular cylindrical tank was attached to the structure. A water solution with white watercolors of 0.28% concentration was used as a test liquid so that the light of a laser sensor could be reflected on the liquid surface. A laser sensor S_1 measured the displacement z_0 of the structure. In the experiments, the direction of the diametric nodal line of the (1, 1) sloshing mode did not necessarily coincide with the y-axis or the x-axis. Because of this reason, the elevation η of the water surface was calculated by the square root of the sum of amplitudes, which were measured by the laser sensors S_2 and S_3 just over the x- and y-axis, respectively (see the top view).

The dimensions of the experimental apparatuses A–E are demonstrated in Table 1. In each apparatus, the relationship, $p_0 \cong 2p_{11}$, was satisfied by adjusting the mass m and the spring constant k of the structure. Here, p_0 is given by $1/(2\pi)\sqrt{k/(m+m_l)}$ Hz, and p_{11} by $1/(2\pi)\sqrt{g\lambda_{11}\tanh(\lambda_{11}h)}$ Hz. The value of the damping coefficient c of the structure was identified by curve-fitting with the theoretical resonance curve given by Eq. (17a) and the values of the damping ratios ζ_{mn} of the water sloshing were identified by curve-fitting with the theoretical resonance curve for the nonlinear-coupled system.

The values of lower natural frequencies for sloshing modes are presented for $h = 60$ mm in Appendix C. Although some internal resonances, for example $2p_{11} \cong p_{02} \cong p_{22}$, exist besides a one-to-two internal resonance $p_0 \cong 2p_{11}$, they cannot appear unless the magnitude of excitation amplitude is considerably large. This was verified by the experimental results in the next section.

Table 1
Dimensions of apparatuses A, B, C, D and E

Apparatus	A	B	C	D	E
Structure mass: m (kg)	7.326	6.265	8.399	7.726	8.326
Spring constant: k (N/m)	9476	4612	4632	9400	9386
Damping coefficient: c (Ns/m)	3.06	1.603	2.06	3.08	3.33
Tank radius: R (mm)	60	85	85	60	60
Water depth: h (mm)	72	45	32	72	72
Water mass: m_l (kg)	0.815	1.019	0.726	0.815	0.815
Damping ratios: ζ_{mn}	0.0085	0.0053	0.0053	0.0085	0.0085
Force: F_0 (N)	0.435	0.165	0.164	0.418	0.488
Position of sensor S_2: x (mm)	50	65	65	50	50
Position of sensor S_3: y (mm)	50	65	65	50	50
Natural frequency: p_0 (Hz)	5.430	4.005	3.586	5.280	5.100
Natural frequency: p_{11} (Hz)	2.727	2.009	1.796	2.727	2.727
Detuning: σ_{11} ($\equiv p_0 - 2p_{11}$) (Hz)	−0.024	−0.013	−0.006	−0.174	−0.354

5. Experimental results

Figs. 17(a) and (b) show a comparison between the experimental and theoretical resonance curves for the structure and the water surface in apparatus A (where the liquid level is high: $h/R = 1.2$), respectively. In this case, $\sigma_{11}(\equiv p_0 - 2p_{11}) = -0.024\,\mathrm{Hz}$, hence, $\sigma_{11}/p_{11} = -0.0088$ in a dimensionless form. Therefore, the relationship $p_0 = 2p_{11}$ nearly holds. The symbol ○ and the symbol • represent the maximum amplitude of an experimental time history of z_0 in the coupled system and the system where the water is replaced by the same mass of the solid body, respectively. Horizontal or oblique arrows represent the direction of changing the excitation frequency. Vertical arrows shown in the figures represent the appearance of jump phenomena in the amplitudes. In these figures a jump phenomenon occurs at the points B'_1 and B'_2 with the gradually increasing of the excitation frequency. As the excitation frequency was gradually decreased stepwise, amplitudes jumped down from the points E'_1 and E'_2. Because the damping due to wetting of the side walls is very sensitive, as mentioned in Ref. [32], the liquid sloshing may reach inside the unstable region and it possibly occur on branch P in Fig. 17(b). The theoretical resonance curves, plotted in Fig. 17, represent the same definitions as discussed in the theoretical analysis. It was observed that the theoretical resonance curves were analogous with the experimental data.

Figs. 18 and 19 show the resonance curves obtained in apparatuses B and C, respectively. The water depth is $h/R = 0.529$ (with $h = 45\,\mathrm{mm}$ and $R = 85\,\mathrm{mm}$) in apparatus B, while $h/R = 0.376$ (with $h = 32\,\mathrm{mm}$ and $R = 85\,\mathrm{mm}$) in apparatus C. Both of the theoretical resonance curves are consistent with the experimental data. Regarding the experimental resonance curves for the water surface, the inclination of the resonance curve changed from the left-hand side to the right-hand side as the water level is decreased—which is also observed in the theoretical result.

Fig. 20 shows the resonance curves for apparatus D, where only the mass m of the structure is increased from the case for apparatus A to examine a deviation of the tuning condition. In this apparatus, $\sigma_{11} = -0.174\,\mathrm{Hz}$ (hence, $\sigma_{11}/p_{11} = -0.0638$). The unstable interval GH appears in the corresponding theoretical resonance curves. In the experiment, amplitude- and phase-modulated motions (designated as APM [Amplitude- and Phase-Modulated motion], and plotted in the symbol ◒) occurred at nearly the same interval as the theoretical one. Figs. 21(a) and (b) show

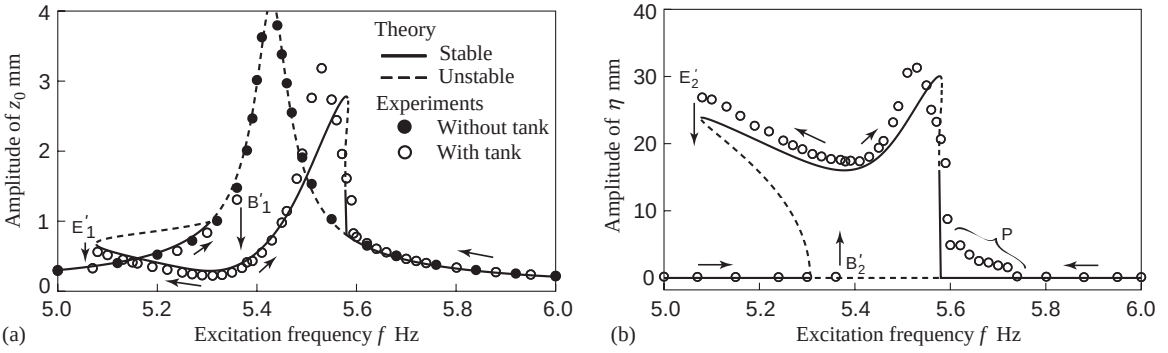

Fig. 17. A comparison between the theoretical and experimental resonance curves for apparatus A when $h/R = 1.2$: (a) amplitudes of z_0; (b) amplitudes of η.

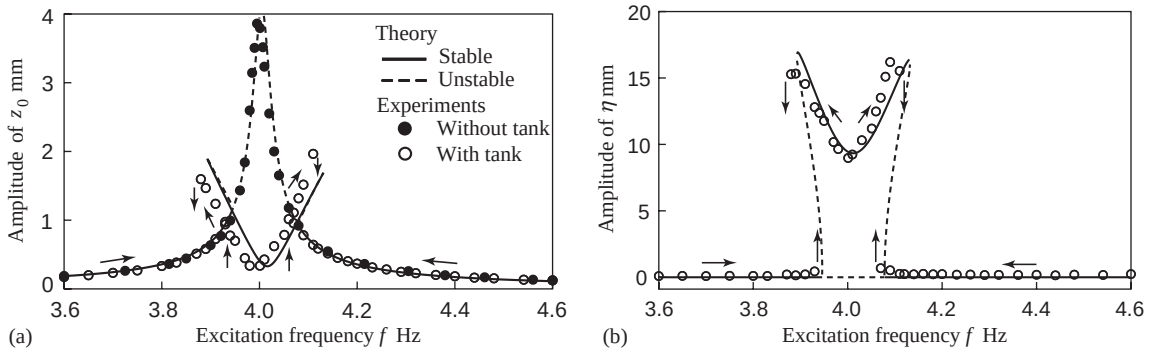

Fig. 18. A comparison between the theoretical and experimental resonance curves for apparatus B when $h/R = 0.529$: (a) amplitudes of z_0; (b) amplitudes of η.

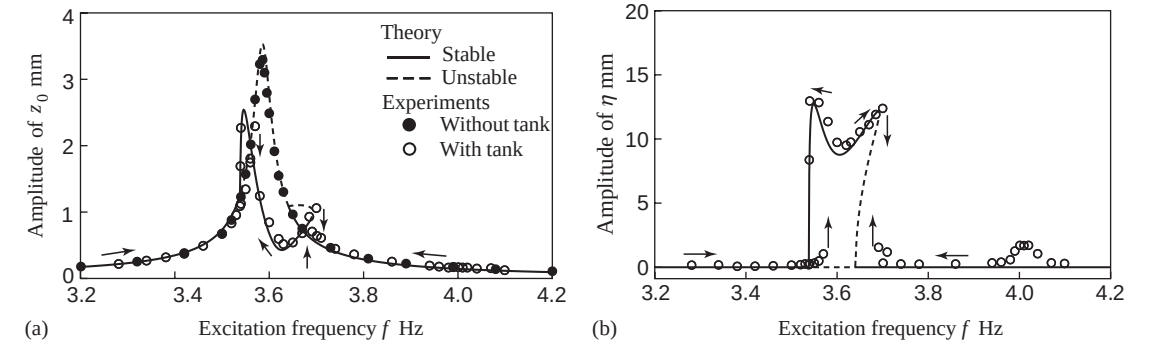

Fig. 19. A comparison between the theoretical and experimental resonance curves for apparatus C when $h/R = 0.376$: (a) amplitudes of z_0; (b) amplitudes of η.

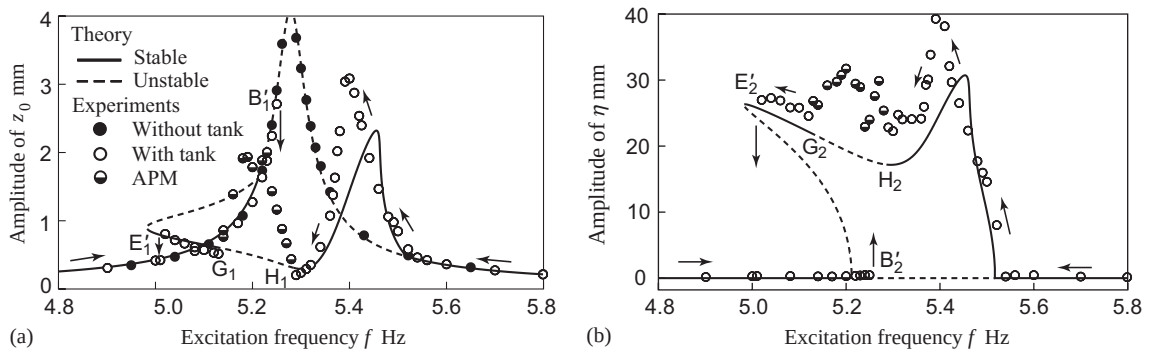

Fig. 20. A comparison between the theoretical and experimental resonance curves for apparatus D when $h/R = 1.2$ and $\sigma_{11} = -0.174$ Hz (i.e., $\sigma_{11}/p_{11} = -0.0638$): (a) amplitudes of z_0; (b) amplitudes of η.

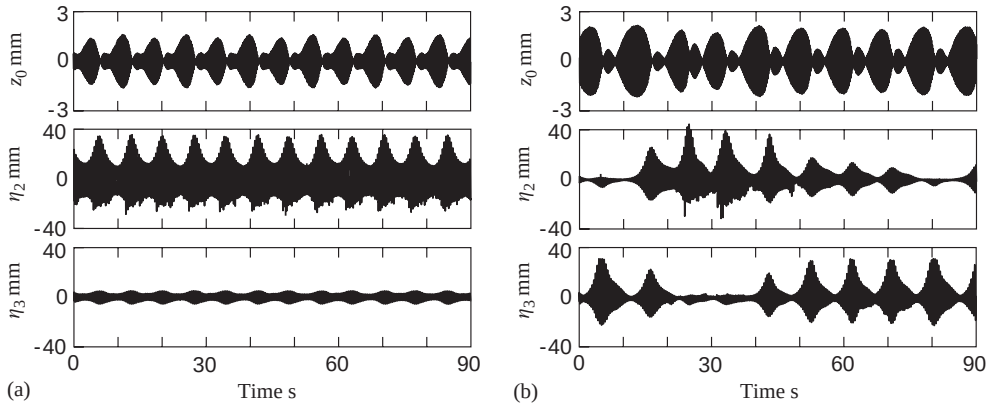

Fig. 21. Time histories for an amplitude- and phase-modulated motion obtained in Fig. 20: (a) $f = 5.170$ Hz; (b) $f = 5.211$ Hz.

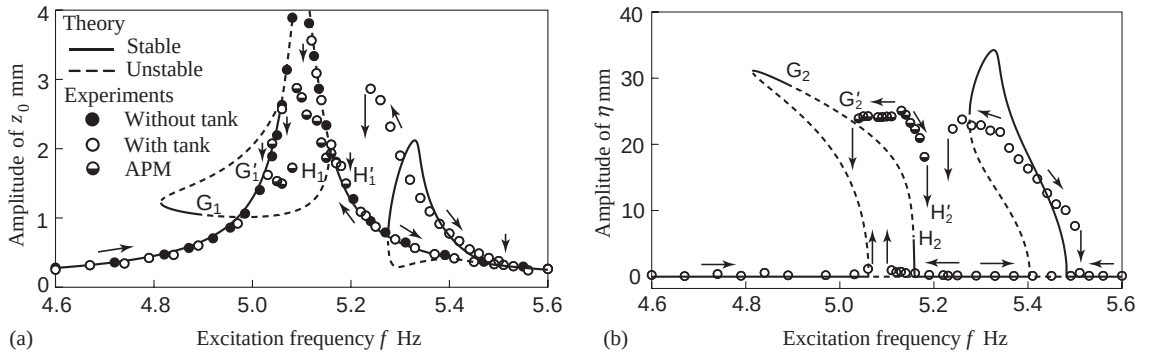

Fig. 22. A comparison between the theoretical and experimental resonance curves for apparatus E when $h/R = 1.2$ and $\sigma_{11} = -0.354$ Hz (i.e., $\sigma_{11}/p_{11} = -0.130$): (a) amplitudes of z_0; (b) amplitudes of η.

the steady-state time histories of amplitude- and phase-modulated motions at $f = 5.170$ and 5.211 Hz, obtained in Fig. 20, respectively. Time histories z_0, η_2 and η_3 were measured by the sensors S_1, S_2 and S_3, correspondingly. It is found that the amplitudes of their envelopes change with a moderate regularity in Fig. 21(a) and irregularly in Fig. 21(b). Fig. 21(b) exhibits a chaotic vibration. These results are quite similar to those of the numerical simulation as in Figs. 10(a) and (c). The occurrence of amplitude and phase modulation in Fig. 21 was not due to the liquid swirling motion because the time histories of η_2 and η_3 were always in phase, as discussed in Section 3.2.

Fig. 22 shows the resonance curves for apparatus E, where the detuning is larger than that for apparatus D. In this apparatus, $\sigma_{11} = -0.354$ Hz (hence, $\sigma_{11}/p_{11} = -0.130$), and thus the deviation of the tuning condition is comparatively large. Amplitude- and phase-modulated motions occur in the interval G′H′. This interval nearly coincides with the theoretical interval GH. In addition, it is found that the nonlinear-coupled vibrations occur in two separated regions of the excitation frequency f.

6. Conclusions

Nonlinear-coupled vibrations of an elastic structure subjected to the vertical sinusoidal excitation with a circular cylindrical liquid container have been investigated. The results can be summarized as follows:

(1) Harmonic oscillations and $\frac{1}{2}$-order subharmonic oscillations occur in the structure and on the liquid surface, respectively, if the relationship between the natural frequencies of the structure and the anti-symmetric sloshing mode is 2:1.

(2) The inclination of the resonance curve for the liquid surface changes from a left-hand side to a right-hand side as the liquid level decreases.

(3) The influence of the detuning parameter defined by $\sigma_{11} \equiv p_0 - 2p_{11}$ is as follows: The amplitude- and phase-modulated motion appears for $\sigma_{11} \leqslant \sigma_{S1} < 0$ when the liquid level is high and for $\sigma_{11} \geqslant \sigma_{S2} > 0$ when the liquid level is low.

(4) Amplitude- and phase-modulated motions exhibit both the regular and irregular changes of the envelope as the excitation frequency changes. The latter change shows the chaotic vibration.

(5) When detuning is comparatively large, the nonlinear-coupled vibrations occur separately in two intervals of the excitation frequency.

(6) In the experiments, it is confirmed that the theoretical resonance curves are quantitatively in agreement with the experimental data. Amplitude- and phase-modulated motions including a chaotic behavior are observed, and the location of their appearance coincides well with the theoretical results.

Acknowledgements

This paper was partially supported by grant-in-aid for Scientific Research from the Japanese Ministry of Education, Culture, Sports, Science and Technology. The authors would like to express their appreciation for their generous support. In addition, the authors thank Professor R. A. Ibrahim of Wayne State University for his valuable comments and suggestions.

Appendix A. Nonlinear terms in Eqs. (22) and (23)

The nonlinear terms G_i $(i = 1, 2, \ldots, 13)$ in Eqs. (22) and (23) are expressed by

$$G_1 = Q_3(a_{11}^2 + b_{11}^2),$$

$$\begin{aligned} G_2 = {} & Q_4\dot{a}_{01}c_{11} + Q_5\dot{a}_{11}c_{01} + Q_6\dot{a}_{11}c_{21} + Q_7\dot{a}_{21}c_{11} + Q_8\dot{b}_{11}d_{21} + Q_9\dot{b}_{21}d_{11} \\ & + Q_{10}(3\dot{a}_{11}c_{11}^2 + \dot{a}_{11}d_{11}^2 + 2\dot{b}_{11}c_{11}d_{11}) + Q_{11}a_{01}a_{11} + Q_{12}(a_{11}a_{21} + b_{11}b_{21}) \\ & + Q_{13}a_{11}^2c_{11} + Q_{14}b_{11}^2c_{11} + Q_{15}a_{11}b_{11}d_{11}, \\ G_3 = {} & Q_{16}\dot{a}_{01}d_{11} + Q_{17}\dot{b}_{11}c_{01} + Q_{18}\dot{a}_{11}d_{21} + Q_{19}\dot{a}_{21}d_{11} + Q_{20}\dot{b}_{11}c_{21} + Q_{21}\dot{b}_{21}c_{11} \\ & + Q_{22}(2\dot{a}_{11}c_{11}d_{11} + \dot{b}_{11}c_{11}^2 + 3\dot{b}_{11}d_{11}^2) + Q_{23}a_{01}b_{11} + Q_{24}(a_{11}b_{21} - a_{21}b_{11}) \\ & + Q_{25}a_{11}b_{11}c_{11} + Q_{26}a_{11}^2d_{11} + Q_{27}b_{11}^2d_{11}, \end{aligned}$$

$$
\begin{aligned}
G_4 &= Q_{28}a_{01}c_{11} + Q_{29}a_{11}c_{01} + Q_{30}(a_{11}c_{21} + b_{11}d_{21}) + Q_{31}(a_{21}c_{11} + b_{21}d_{11}) \\
&\quad + Q_{32}a_{11}c_{11}^2 + Q_{33}b_{11}c_{11}d_{11} + Q_{34}a_{11}d_{11}^2, \\
G_5 &= Q_{35}a_{01}d_{11} + Q_{36}b_{11}c_{01} + Q_{37}(a_{11}d_{21} - b_{11}c_{21}) + Q_{38}(a_{21}d_{11} - b_{21}c_{11}) \\
&\quad + Q_{39}b_{11}c_{11}^2 + Q_{40}a_{11}c_{11}d_{11} + Q_{41}b_{11}d_{11}^2, \\
G_6 &= Q_{42}(\dot{a}_{11}c_{11} + \dot{b}_{11}d_{11}) + Q_{43}(a_{11}^2 + b_{11}^2), \quad G_7 = Q_{44}(\dot{a}_{11}c_{11} + \dot{b}_{11}d_{11}) + Q_{45}(a_{11}^2 + b_{11}^2), \\
G_8 &= Q_{46}(a_{11}c_{11} + b_{11}d_{11}), \quad G_9 = Q_{47}(\dot{a}_{11}c_{11} - \dot{b}_{11}d_{11}) + Q_{48}(a_{11}^2 - b_{11}^2), \\
G_{10} &= Q_{47}(\dot{a}_{11}d_{11} + \dot{b}_{11}c_{11}) + Q_{48}a_{11}b_{11}, \quad G_{11} = Q_{49}(a_{11}c_{11} - b_{11}d_{11}), \\
G_{12} &= Q_{49}(a_{11}d_{11} + b_{11}c_{11}), \\
G_{13} &= Q_{50}(\dot{a}_{11}c_{11} + \dot{b}_{11}d_{11}) + Q_{51}(a_{11}^2 + b_{11}^2),
\end{aligned} \tag{A.1}
$$

where the coefficients Q_i $(i = 1, 2, \ldots, 51)$ are given by

$$
\begin{aligned}
&Q_1 = v_1 + \pi v_2 h, \quad Q_2 = -\pi v_2, \quad Q_3 = -\frac{\pi v_2 \alpha}{2\cosh^2(\xi_{11}h)}, \quad Q_4 = \psi_{01}K_1^{120}, \\
&Q_5 = \psi_{11}K_1^{120}, \quad Q_6 = \tfrac{1}{2}\psi_{11}K_1^{021}, \quad Q_7 = \tfrac{1}{2}\psi_{21}K_1^{021}, \quad Q_8 = Q_6, \quad Q_9 = Q_7, \\
&Q_{10} = \tfrac{1}{8}\xi_{11}^2 K_1^{040}, \quad Q_{11} = \gamma_1^{101} + \psi_{01}\psi_{11}K_1^{120}, \quad Q_{12} = \tfrac{1}{2}(\gamma_1^{112} + 2\kappa_1^{021} + \psi_{11}\psi_{21}K_1^{021}), \\
&Q_{13} = \tfrac{1}{4}\psi_{11}(3\Gamma_1^{1111} + \kappa_1^{040} + 3\xi_{11}^2 K_1^{040}), \quad Q_{14} = \tfrac{1}{4}\psi_{11}(\Gamma_1^{1111} + 3\kappa_1^{040} + \xi_{11}^2 K_1^{040}), \\
&Q_{15} = \tfrac{1}{2}\psi_{11}(\Gamma_1^{1111} - \kappa_1^{040} + \xi_{11}^2 K_1^{040}), \quad Q_{16} = Q_4, \quad Q_{17} = Q_5, \quad Q_{18} = Q_6, \quad Q_{19} = -Q_7, \\
&Q_{20} = -Q_8, \quad Q_{21} = Q_9, \quad Q_{22} = Q_{10}, \quad Q_{23} = Q_{11}, \quad Q_{24} = Q_{12}, \quad Q_{25} = Q_{15}, \\
&Q_{26} = Q_{14}, \quad Q_{27} = Q_{13}, \quad Q_{28} = \gamma_1^{101} - \xi_{01}^2 K_1^{120}, \quad Q_{29} = \gamma_1^{101} - \xi_{11}^2 K_1^{120}, \\
&Q_{30} = \tfrac{1}{2}(\gamma_1^{112} + 2\kappa_1^{021} - \xi_{11}^2 K_1^{021}), \quad Q_{31} = \tfrac{1}{2}(\gamma_1^{112} + 2\kappa_1^{021} - \xi_{21}^2 K_1^{021}), \\
&Q_{32} = \tfrac{1}{8}\psi_{11}(6\Gamma_1^{1111} + 2\kappa_1^{040} - 3\xi_{11}^2 K_1^{040}), \quad Q_{33} = \tfrac{1}{4}\psi_{11}(2\Gamma_1^{1111} + 2\kappa_1^{040} - \xi_{11}^2 K_1^{040}), \\
&Q_{34} = \tfrac{1}{8}\psi_{11}(2\Gamma_1^{1111} - 2\kappa_1^{040} - \xi_{11}^2 K_1^{040}), \quad Q_{35} = Q_{28}, \quad Q_{36} = Q_{29}, \quad Q_{37} = Q_{30}, \\
&Q_{38} = -Q_{31}, \quad Q_{39} = Q_{34}, \quad Q_{40} = Q_{33}, \quad Q_{41} = Q_{32}, \quad Q_{42} = \psi_{11}G_{11}, \\
&Q_{43} = \tfrac{1}{2}(\alpha + g_{11} + \psi_{11}^2 G_{11}), \\
&Q_{44} = \tfrac{1}{2}\psi_{11}K_0^{120}, \quad Q_{45} = \tfrac{1}{4}(\gamma_0^{011} + \kappa_0^{120} + \psi_{11}^2 K_0^{120}), \\
&Q_{46} = \tfrac{1}{2}(\gamma_0^{011} + \kappa_0^{120} - \xi_{11}^2 K_0^{120}), \\
&Q_{47} = \tfrac{1}{2}\psi_{11}K_2^{021}, \quad Q_{48} = \tfrac{1}{4}(\gamma_2^{211} - \kappa_2^{021} + \psi_{11}^2 K_2^{021}), \\
&Q_{49} = \tfrac{1}{2}(\gamma_2^{211} - \kappa_2^{021} - \xi_{11}^2 K_2^{021}), \\
&Q_{50} = -Q_2 Q_{42}, \quad Q_{51} = Q_3 - Q_2 Q_{43}.
\end{aligned} \tag{A.2}
$$

The symbols in Eq. (A.2) are as follows:

$$
G_{m1} = \int_0^1 r J_m^2(\xi_{m1}r)\,\mathrm{d}r, \quad g_{m1} = \int_0^1 \frac{1}{r} J_m^2(\xi_{m1}r)\,\mathrm{d}r,
$$

$$
\begin{aligned}
K_m^{ijk} &= \int_0^1 rJ_0^i(\xi_{01}r)\ J_1^j(\xi_{11}r)\ J_2^k(\xi_{21}r)\,\mathrm{d}r/G_{m1},\\
\alpha &= \int_0^1 r\left\{\frac{\mathrm{d}J_1(\xi_{11}r)}{\mathrm{d}r}\right\}^2\mathrm{d}r = \tfrac{1}{4}\xi_{11}^2\int_0^1 r\{J_0(\xi_{11}r)-J_2(\xi_{11}r)\}\,\mathrm{d}r,\\
\kappa_m^{ijk} &= \int_0^1 \frac{1}{r}J_0^i(\xi_{01}r)J_1^j(\xi_{11}r)J_2^k(\xi_{21}r)\,\mathrm{d}r/G_{m1},\\
\Gamma_m^{ijkl} &= \int_0^1 rJ_i(\xi_{i1}r)\ J_j(\xi_{j1}r)\frac{\mathrm{d}}{\mathrm{d}r}[J_k(\xi_{k1}r)]\frac{\mathrm{d}}{\mathrm{d}r}[J_l(\xi_{l1}r)]\,\mathrm{d}r/G_{m1},\\
\gamma_m^{ijk} &= \int_0^1 rJ_i(\xi_{i1}r)\frac{\mathrm{d}}{\mathrm{d}r}[J_j(\xi_{j1}r)]\frac{\mathrm{d}}{\mathrm{d}r}[J_k(\xi_{k1}r)]\,\mathrm{d}r/G_{m1},\\
\psi_{mn} &= \xi_{mn}\tanh(\xi_{mn}h).
\end{aligned}
\tag{A.3}
$$

Appendix B. Nonlinear terms in Eq. (24)

The nonlinear terms H_i $(i=1,2,\ldots,6)$ in Eq. (24) are given by

$$
\begin{aligned}
H_1 &= S_1(1+\psi_{11}\ddot{z}_0)(c_{11}^2+d_{11}^2)+S_2(\dot{c}_{11}^2+\dot{d}_{11}^2),\\
H_2 &= S_3\dot{c}_{01}\dot{c}_{11}+S_4(\dot{c}_{11}\dot{c}_{21}+\dot{d}_{11}\dot{d}_{21})+S_5c_{11}\dot{c}_{11}^2+S_6c_{11}\dot{d}_{11}^2+S_7\dot{c}_{11}\dot{d}_{11}d_{11}\\
&\quad+S_8c_{01}c_{11}+S_9c_{11}c_{21}+S_{10}d_{11}d_{21}+S_{11}c_{11}^3+S_{12}c_{11}d_{11}^2,\\
H_3 &= S_{13}\dot{c}_{01}\dot{d}_{11}+S_{14}(\dot{c}_{11}\dot{d}_{21}-\dot{c}_{21}\dot{d}_{11})+S_{15}\dot{c}_{11}^2d_{11}+S_{16}\dot{d}_{11}^2d_{11}+S_{17}c_{11}\dot{c}_{11}\dot{d}_{11}\\
&\quad+S_{18}c_{01}d_{11}+S_{19}c_{11}d_{21}+S_{20}c_{21}d_{11}+S_{21}d_{11}^3+S_{22}c_{11}^2d_{11},\\
H_4 &= S_{23}(1+\psi_{11}\ddot{z}_0)(c_{11}^2+d_{11}^2)+S_{24}(\dot{c}_{11}^2+\dot{d}_{11}^2),\\
H_5 &= S_{25}(1+\psi_{11}\ddot{z}_0)(c_{11}^2-d_{11}^2)+S_{26}(\dot{c}_{11}^2-\dot{d}_{11}^2),\\
H_6 &= S_{27}(1+\psi_{11}\ddot{z}_0)c_{11}d_{11}+S_{28}\dot{c}_{11}\dot{d}_{11},
\end{aligned}
\tag{B.1}
$$

where S_i $(i=1,2,\ldots,28)$ are all constants determined by the system parameters, and they are given as follows:

$$
\begin{aligned}
S_1 &= -Q_{50}/\psi_{11},\quad S_2=Q_{51}/\psi_{11}^2,\quad S_3=Q_{29}/\psi_{11}+(Q_{11}+Q_{28})/\psi_{01},\\
S_4 &= Q_{30}/\psi_{11}+(Q_{12}+Q_{31})/\psi_{21},\\
S_5 &= (Q_{13}+2Q_{32}-Q_4Q_{45}-Q_7Q_{48})/\psi_{11}+Q_{46}(Q_{11}+Q_{28})/(\psi_{11}\psi_{01})\\
&\quad+Q_{49}(Q_{12}+Q_{31})/(\psi_{11}\psi_{21})-(Q_{28}Q_{45}+Q_{31}Q_{48})/\psi_{11}^2,\\
S_6 &= (Q_{14}+Q_{33}-Q_4Q_{45}+Q_7Q_{48})/\psi_{11}+Q_{49}(Q_{12}+Q_{31})/(\psi_{11}\psi_{21})\\
&\quad+(-Q_{28}Q_{45}+Q_{31}Q_{48})/\psi_{11}^2,
\end{aligned}
$$

$$
\begin{aligned}
S_7 &= (Q_{15} + Q_{33} + 2Q_{34} - Q_9Q_{48})/\psi_{11} + Q_{46}(Q_{11} + Q_{28})/(\psi_{11}\psi_{01}) - Q_{31}Q_{48}/\psi_{11}^2,\\
S_8 &= -Q_4 - Q_5 - (Q_{28} + Q_{29})/\psi_{11}, \quad S_9 = -Q_6 - Q_7 - (Q_{30} + Q_{31})/\psi_{11},\\
S_{10} &= -Q_8 - Q_9 - (Q_{30} + Q_{31})/\psi_{11},\\
S_{11} &= -3Q_{10} + Q_4Q_{44} + Q_7Q_{47} + (-Q_{32} + Q_{28}Q_{44} + Q_{31}Q_{47})/\psi_{11},\\
S_{12} &= -3Q_{10} + Q_4Q_{44} + Q_{47}(-Q_7 + 2Q_9) + (-Q_{33} - Q_{34} + Q_{28}Q_{44} + Q_{31}Q_{47})/\psi_{11},\\
S_{13} &= Q_{36}/\psi_{11} + (Q_{23} + Q_{35})/\psi_{01}, \quad S_{14} = Q_{37}/\psi_{11} + (Q_{24} - Q_{38})/\psi_{21},\\
S_{15} &= (Q_{26} + Q_{40} - Q_{16}Q_{45} - Q_{19}Q_{48})/\psi_{11} + Q_{49}(Q_{24} - Q_{38})/(\psi_{11}\psi_{21})\\
&\quad - (Q_{35}Q_{45} + Q_{38}Q_{48})/\psi_{11}^2,\\
S_{16} &= (Q_{27} + 2Q_{41} - Q_{16}Q_{45} + Q_{19}Q_{48})/\psi_{11} + Q_{46}(Q_{23} + Q_{35})/(\psi_{11}\psi_{01})\\
&\quad + Q_{49}(Q_{24} - Q_{38})/(\psi_{11}\psi_{21}) - (Q_{35}Q_{45} - Q_{38}Q_{48})/\psi_{11}^2,\\
S_{17} &= (Q_{25} + 2Q_{39} + Q_{40} - Q_{21}Q_{48})/\psi_{11} + Q_{46}(Q_{23} + Q_{35})/(\psi_{11}\psi_{01}) + Q_{38}Q_{48}/\psi_{11}^2,\\
S_{18} &= -Q_{16} - Q_{17} - (Q_{35} + Q_{36})/\psi_{11}, \quad S_{19} = -Q_{18} - Q_{21} - (Q_{37} - Q_{38})/\psi_{11},\\
S_{20} &= -Q_{19} - Q_{20} + (Q_{37} - Q_{38})/\psi_{11},\\
S_{21} &= -3Q_{22} + Q_{16}Q_{44} - Q_{19}Q_{47} + (-Q_{41} + Q_{35}Q_{44} - Q_{38}Q_{47})/\psi_{11},\\
S_{22} &= -3Q_{22} + Q_{16}Q_{44} + Q_{47}(Q_{19} + 2Q_{21}) - (Q_{39} + Q_{40} - Q_{35}Q_{44} + Q_{38}Q_{47})/\psi_{11},\\
S_{23} &= -(\psi_{01}Q_{44} + Q_{46})/\psi_{11}, \quad S_{24} = (\psi_{01}Q_{45} + \psi_{11}Q_{46})/\psi_{11}^2,\\
S_{25} &= -(\psi_{21}Q_{47} + Q_{49})/\psi_{11}, \quad S_{26} = (\psi_{21}Q_{48} + \psi_{11}Q_{49})/\psi_{11}^2,\\
S_{27} &= -2(\psi_{21}Q_{47} + Q_{49})/\psi_{11},\\
S_{28} &= (\psi_{21}Q_{48} + 2\psi_{11}Q_{49})/\psi_{11}^2.
\end{aligned}
\tag{B.2}
$$

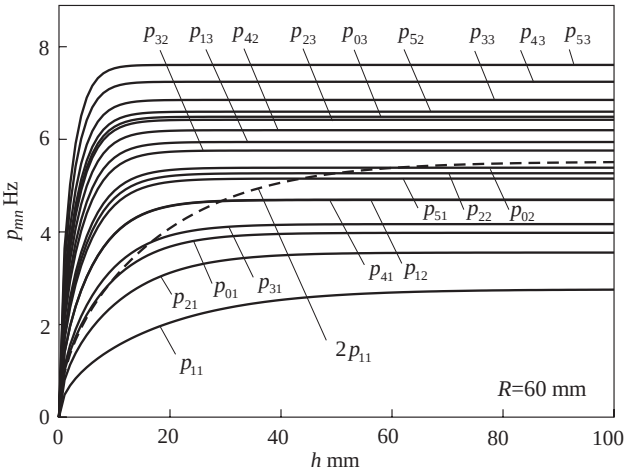

Fig. A1. Natural frequencies for the liquid sloshing for the tank radius $R = 60$ mm.

Appendix C. Natural frequencies for sloshing

The lower natural frequencies for the liquid sloshing for the tank radius $R = 60$ mm is shown in Fig. A1. They are plotted by solid lines. The broken line represents the values of $2p_{11}$. Each natural frequency increases as the liquid level h increases. It is found from this figure that many different natural frequencies are close together. In this case, the value of p_{41} is nearly equal to that of p_{12}. Depending on the parameter values, the relationships of some internal resonances hold besides $p_0 \cong 2p_{11}$.

References

[1] R.A. Ibrahim, V.N. Pilipchuk, T. Ikeda, Recent advances in liquid sloshing dynamics, *Applied Mechanics Reviews* 54 (2) (2001) 133–199.

[2] R.E. Hutton, An investigation of resonant, nonlinear, nonplanar free surface oscillations of a fluid, NASA Technical Note D-1870, 1963, pp. 1–64.

[3] H.N. Abramson, The dynamic behavior of liquids in moving containers, NASA SP-106, 1966.

[4] H.N. Abramson, W.H. Chu, D.D. Kana, Some studies of nonlinear lateral sloshing in rigid containers, *Applied Mechanics* 33 (4) (1966) 777–784.

[5] J.W. Miles, Resonantly forced surface waves in a circular cylinder, *Journal of Fluid Mechanics* 149 (1984) 15–31.

[6] F.G. Dodge, D.D. Kana, H.N. Abramson, Liquid surface oscillations in longitudinal excited rigid cylindrical containers, *AIAA Journal* 3 (4) (1965) 685–695.

[7] H. Takahara, K. Kimura, M. Sakata, Nonlinear axisymmetrical liquid oscillation in a circular cylinder tank subjected to vertical excitation, Preprint of the Japan Society of Mechanical Engineers, No. 930-9 (III), 234–236, 1993 (in Japanese).

[8] K. Kimura, H. Takahara, M. Sakata, Effects of higher order radial modes upon nonlinear sloshing in a circular cylindrical tank subjected to vertical excitation, *Transactions of the JSME C* 60 (578) (1994) 3259–3267 (in Japanese).

[9] K. Senda, N. Nakagawa, On the vibration of an elevated water-tank—I, *Technical Reports of Osaka University* 4 (117) (1954) 247–264.

[10] H. Hagiuda, Oscillation control system exploiting fluid force generated by water sloshing, *Mitsui Zosen Technical Review* 137 (1988) 13–20 (in Japanese).

[11] Y. Fujino, B. Pacheco, C. Piyawat, K. Fujii, An experimental study on tuned liquid damper using circular containers, *Transactions of the Japan Society of Civil Engineers* 34-A (1988) 603–616 (in Japanese).

[12] T. Ikeda, N. Nakagawa, Non-linear vibrations of a structure caused by water sloshing in a rectangular tank, *Journal of Sound and Vibration* 201 (1) (1997) 23–41.

[13] T. Ikeda, T. Hirayama, N. Nakagawa, Nonlinear vibrations of a structure caused by water sloshing in a cylindrical tank, *Transactions of the JSME, International Journal, Series C* 41 (3) (1998) 639–651.

[14] T. Ikeda, Nonlinear vibrations in an elastic structure subjected to vertical excitation and coupled with liquid sloshing in a rectangular tank, in: *Proceedings of the 1997 ASME Design Engineering Technical Conferences*, DETC97/VIB-4096, Sacramento, California, 1977.

[15] R.A. Ibrahim, A.D.S. Barr, Autoparametric resonance in a structure containing a liquid, part I: two mode interaction, *Journal of Sound and Vibration* 42 (2) (1975) 159–179.

[16] R.A. Ibrahim, Multiple internal resonance in a structure–liquid system, *Engineering for Industry* 98 (3) (1976) 1092–1098.

[17] R.A. Ibrahim, J.S. Gau, A. Soundararajan, Parametric and autoparametric vibrations of an elevated water tower, part I: non-linear parametric resonance, *Journal of Sound and Vibration* 121 (3) (1988) 413–428.

[18] T. Ikeda, S. Murakami, Nonlinear vibrations in an elastic structure subjected to vertical excitation and coupled with liquid sloshing in a cylindrical tank (resonance with an axisymmetric mode), in: *Proceedings of the 1999 ASME Design Engineering Technical Conferences*, DETC99/VIB-8048, Las Vegas, Nevada, 1999.
[19] J.J. Stoker, *Nonlinear Vibrations*, Wiley, New York, 1950.
[20] M. Sakata, K. Kimura, M. Utsumi, Non-stationary response of non-linear liquid motion in a cylindrical tank subjected to random base excitation, *Journal of Sound and Vibration* 94 (3) (1984) 351–363.
[21] T. Ikeda, R.A. Ibrahim, Nonlinear random responses of a structure parametrically coupled with liquid sloshing in a cylindrical tank, *Journal of Sound and Vibration* 284 (1–2) (2005) 75–102; doi:10.1016/j.jsv.2004.06.049.
[22] T. Ikeda, Nonlinear vibrations in a parametrically excited fluid–structure interaction system with one-to-one internal resonance, in: *Proceedings of the 2003 ASME International Mechanical Engineering Congress & Exposition*, IMECE2003-43996, Washington, DC, 2003.
[23] H. Hatwal, A.K. Mallik, A. Ghosh, Forced nonlinear oscillations of autoparametric system, part 2: chaotic responses, *Applied Mechanics* 50 (3) (1983) 663–668.
[24] B. Banerjee, A.K. Bajaj, P. Davies, Resonant dynamics of an autoparametric system: a study using higher-order averaging, *International Journal of Non-Linear Mechanics* 31 (1) (1996) 21–39.
[25] A.K. Bajaj, S.I. Chang, J.M. Johnson, Amplitude modulated dynamics of a resonantly excited autoparametric two degree-of-freedom system, *Nonlinear Dynamics* 5 (4) (1994) 433–457.
[26] A.H. Nayfeh, On the undesirable roll characteristics of ships in regular seas, *Journal of Ship Research* 32 (2) (1988) 92–100.
[27] B. Balachandran, A.H. Nayfeh, Observations of modal interactions in resonantly forced beam-mass structures, *Nonlinear Dynamics* 2 (2) (1991) 77–117.
[28] B. Balachandran, A.H. Nayfeh, Nonlinear motions of beam-mass structure, *Nonlinear Dynamics* 1 (1) (1990) 39–61.
[29] B. Balachandran, A.H. Nayfeh, Cyclic motions near a Hopf bifurcation of a four-dimensional system, *Nonlinear Dynamics* 3 (1) (1992) 19–39.
[30] E.J. Doedel, A.R. Champneys, T.F. Fairgrieve, Y.A. Kuznetsov, B. Sandstede, X. Wang, *AUTO97: continuation and bifurcation software for ordinary differential equations* (with HomCont), 1977 Concordia University, Canada, 1977.
[31] A. Wolf, J.B. Swift, H.L. Swinney, J.A. Vastano, Determining Lyapunov exponents from a time series, *Physica* 16D (1895) 285–317.
[32] K.M. Case, W.C. Parkinson, Damping of surface waves in an incompressible liquid, *Journal of Fluid Mechanics* 2 (1957) 172–184.